

## COMPARISON OF EARTHQUAKE LOCATIONS DETERMINED WITH DATA FROM A NETWORK OF STATIONS AND SMALL TRIPARTITE ARRAYS ON KILAUEA VOLCANO, HAWAII\*

BY PETER L. WARD AND SOREN GREGERSEN

### ABSTRACT

The hypocenters of 43 earthquakes on Kilauea Volcano were analyzed in detail in order to examine the accuracy of hypocenters determined with data from tripartite arrays and to look for evidence of zones of abnormally high or low velocity in a region of complex crustal structure. Ten vertical and two horizontal seismometers were operated on the south flank of Kilauea within the seismic network of the Hawaiian Volcano Observatory. A number of combinations of the temporary stations were treated as separate tripartite arrays. The sides of each tripartite array were 1 to 2 km long. Azimuths and apparent velocities of *P*-wave fronts observed at these arrays generally agreed well with the values predicted from hypocenters calculated using data from as many as 20 stations. Some observed azimuths differed from the predicted values by over 40° and some apparent velocities differed by nearly a factor of 2. These differences are consistent with the travel-time residuals found when the hypocenters are located with all available data. They can be attributed to local zones of abnormally high or low velocity or to changes in the thicknesses of the assumed crustal layers. Waves that travel through the east and southwest rift zones arrive relatively early and the waves traveling through the Kaoiki fault zone arrive late. Refraction data were compiled to obtain a new average crustal structure. When small tripartite arrays are used to locate shallow earthquakes, a crustal structure with a linear increase in velocity should be assumed in order to calculate unique hypocenters and to obtain less scatter in a group of hypocenters.

### INTRODUCTION

Hypocenters of local earthquakes are usually calculated most accurately with data from a network of seismometers spaced throughout the epicentral region. Often, however, logistical problems and available equipment limit the number of possible seismograph sites. Perhaps the most compact and economical network is a tripartite array consisting of one recorder that receives data from three seismometers spaced 1 or 2 km apart. Such an array, when used with care, can often provide a reasonable alternative to a large network of stations for locating hypocenters and has been used by many workers (for example, Asada and Suzuki, 1950; Matumoto, 1959; Miyamura *et al.*, 1964; Matumoto and Ward, 1967; Stauder and Ryall, 1967). A small tripartite array also provides data on apparent velocity and azimuth of wave approach, making it useful for studying lateral refraction of waves in complex crustal structures (for example, Aki, 1962; Aki and Matumoto, 1963; Otsuka, 1966, Ohtake *et al.*, 1965; Mikumo, 1965; Oike and Mikumo, 1968). A tripartite array, which is generally more portable than a network, can be used effectively for short field programs.

During August and September 1967, three tripartite arrays were operated on the south flank of Kilauea, the most active volcano on the Island of Hawaii (Figure 1). The three

\* Publication Authorized by the Director, U.S. Geological Survey.

arrays (N, E, and W) were placed so that their stations together with a central station could be combined into other tripartite arrays of varying geometry and size. All ten of these stations, collectively referred to as the array, were placed in the middle of a network of ten stations operated by the staff of the Hawaiian Volcano Observatory of the U.S. Geological Survey. The objectives of this work were, first, to evaluate the accuracy of locations determined with data from these tripartite arrays with respect to locations

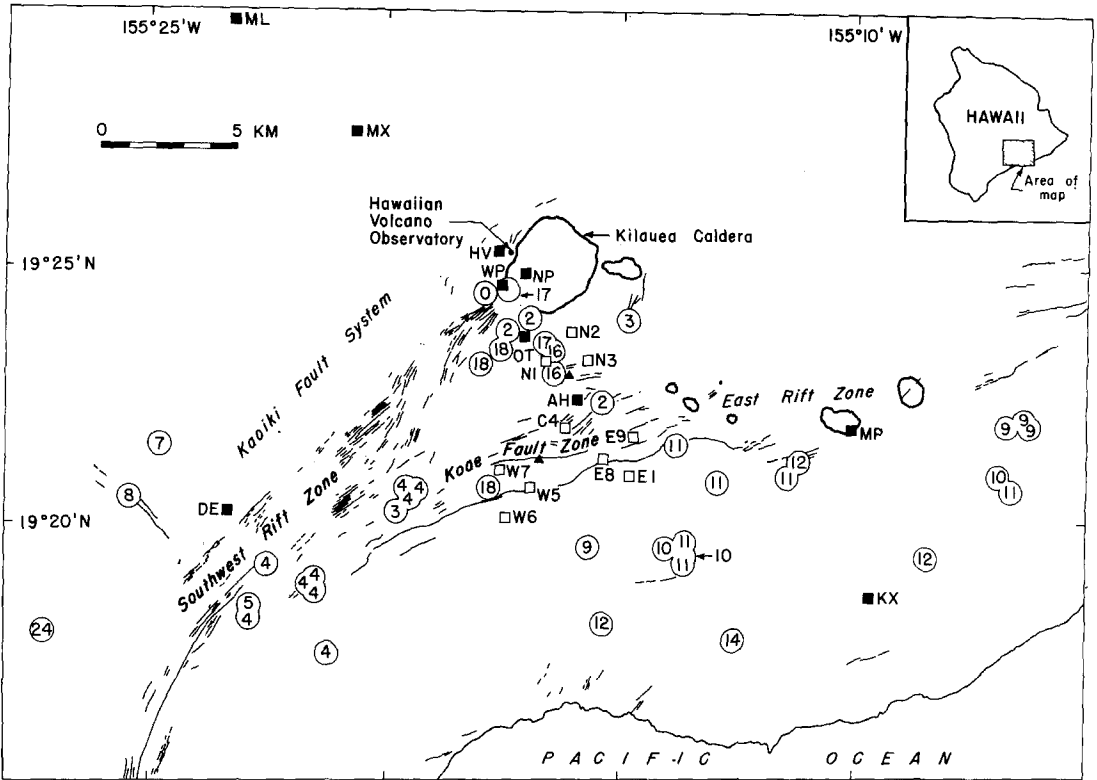


FIG. 1. Map of Kilauea Volcano showing the location of seismic stations and earthquakes used in this study. Hypocenters are shown by circles containing numbers for depth. The lines designate fractures, fissures, and faults. Open and solid squares represent the temporary array stations and the previously existing network seismic stations, respectively. Triangles represent triangulation bench marks used to locate and orient the array.

determined from the network data and, second, to look for evidence of lateral refraction in a region where rocks with relatively high velocities might be expected to occur in narrow zones near the surface. These objectives are approached by first deriving a reasonable crustal structure. Then the network and array data are combined to determine precise locations of 43 earthquakes. Many of the assumptions made in the standard methods of locating earthquakes are evaluated in order to assess the precision and accuracy of these hypocenters and of hypocenters in Hawaii routinely reported by the Hawaiian Volcano Observatory. Finally, the tripartite array and network solutions are compared to demonstrate some of the benefits and problems of using tripartite arrays. Evidence is found for slightly higher than normal crustal velocities along the rift zones and slightly lower than normal crustal velocities near the Koaie fault zone. Focal mechanisms are determined for some of the earthquakes, and one of these mechanism solutions turns out to be very dependent on the crustal structure assumed. The problems and errors involved in using tripartite arrays are outlined in the appendix. Several authors have misused

data from tripartite arrays either because they failed to adequately consider special problems with refracted waves or they did not properly assess the possible errors in hypocentral locations.

The term "precision" of a hypocentral location as used here is a measure of how well one hypocenter is located relative to others determined by the same method. The precision is primarily influenced by errors in timing, errors in the location of the stations, clarity of the first arrivals, and other parameters. In this study, errors in timing the *P*-wave arrivals have the greatest effect. The "accuracy" of a hypocentral location, in contrast to the precision, is a measure of how closely the calculated hypocenter approximates the true hypocenter. The accuracy is usually worse than the precision and is influenced primarily by imperfect knowledge of the crustal structure in three dimensions between the hypocenter and each of the stations. The most direct method for determining the accuracy is to detonate explosions near each hypocenter.

#### INSTRUMENTATION AND TIMING ERRORS

The ten vertical-component geophones of the array installed for this project were connected by cables of up to one mile in length to four magnetic tape recorders. Similar instruments are described by Eaton *et al.*, (1970). The geophones sites are shown in Figure 1. Site C4 also contained two horizontal-component instruments. These ten seismometer sites, listed at the beginning of Table 1, are referred to collectively in this paper as the array. The network, as used here, refers to the last ten seismometer sites listed in Table 1. Data from these stations were transmitted by cable to the Hawaiian Volcano Observatory and recorded on a Develocorder as described by Endo (1971). The observatory clock was connected to the Develocorder and by long cables to each of the tape recorders so that the relative time was the same on all recorders. Time corrections were added for delays of 0.035 sec introduced by relays in the timing lines. To test the timing errors, *P*-wave arrival times for selected earthquakes were read several dozen times each. The standard deviation of a reading was found to be only 0.003 sec for the array records, once it is decided where to pick the beginning or the first peak or trough of the wave. The

TABLE 1: STATION LOCATIONS AND STATION TRAVEL-TIME CORRECTIONS FOR EARTHQUAKES FROM DIFFERENT REGIONS. THE STATION CORRECTIONS INCLUDE THE ELEVATION CORRECTIONS FOR  $v=5.1$

NAME	LATITUDE (DEG) (MIN)	LONGITUDE (DEG) (MIN)	ELEVATION (METERS)	ELEVATION CORRECTIONS		STATION CORRECTIONS			
				$v=3.1$	$v=5.1$	DEEP	SW	SE	
<b>ARRAY STATIONS</b>									
N1	19 23.19	155 16.53	1087	0.02	0.01	0.03	0.03	0.06	
N2	19 23.73	155 16.03	1119	0.03	0.02	0.04	-0.01	0.06	
N3	19 23.21	155 15.72	1098	0.02	0.02	0.03	0.02	0.04	
E8	19 21.27	155 15.32	1015	0.00	0.00	0.01	-0.03	-0.03	
E9	19 21.72	155 14.71	1011	0.00	0.00	0.06	0.00	-0.01	
E1	19 20.93	155 17.75	983	-0.01	-0.01	0.01	-0.02	-0.05	
W5	19 20.69	155 16.86	979	-0.01	-0.01	0.08	0.02	0.00	
W6	19 20.10	155 17.39	931	-0.03	-0.02	0.07	0.06	0.02	
W7	19 21.03	155 17.52	989	-0.01	-0.01	0.05	0.05	0.00	
C4	19 21.87	155 16.15	1021	0.00	0.00	0.02	-0.01	-0.01	
<b>NETWORK STATIONS</b>									
ML	19 29.8	155 23.3	2010	0.30	0.19	0.26	0.26		
MX	19 27.6	155 20.7	1475	0.14	0.09	0.24	0.24		
AH	19 22.4	155 15.9	1070	0.02	0.01	0.06	-0.02	0.02	
UT	13 23.4	155 16.8	1084	0.02	0.01	0.04	-0.01	0.05	
DE	19 20.2	155 23.3	815	-0.06	-0.04	-0.13	-0.03	-0.01	
NP	19 24.9	155 17.0	1115	0.03	0.02	-0.12	-0.08	-0.04	
WP	19 24.7	155 17.5	1115	0.03	0.02	-0.07	-0.05	-0.01	
MP	19 21.8	155 10.0	886	-0.05	-0.03	-0.14		-0.08	
KX	19 18.5	155 9.6	201	-0.25	-0.16	-0.15		-0.12	
HV	19 25.4	155 17.6	1240	0.07	0.04	-0.07	0.00	0.09	

main inaccuracy, however, is in picking the same part of the *P* wave on all stations. The standard error is estimated to be about 0.005 to 0.01 sec for the array stations and about 0.02 sec for the network stations. To obtain such precision, the Develocorder films were projected onto a digitizing table, which has a resolution of 0.1 mm, at a scale of about 23 mm/sec.

Array locations, relative to two triangulation bench marks within the array, were surveyed with transit, geodimeter, and altimeter. The distances between seismometers in the array are known to about 5 meters. The location of each seismometer in the array (Table 1) is known to  $\pm 0.01$  min in latitude and longitude and  $\pm 5$  meters in elevation. Network site locations were determined by locating the station on a contour map (scale 1:50,000) (R. Koyanagi, personal communication, 1971). Errors in locations of these stations are estimated to be  $\pm 0.1$  min in latitude and longitude and  $\pm 50$  meters in elevation. In the data analysis, arrivals at different vertical seismometers in the array were combined in several groups of three, allowing evaluation of data from a number of different tripartite arrays with varying geometry, size, and location.

The array stations are spaced to the north and south and in the middle of the Koae Fault zone (Figure 1), a region of tension cracks, normal faults, and grabens but with few eruptive fissures. Many of the network stations lie near the east or southwest Rifts and near the summit of Kilauea (Figure 1), which are regions with numerous eruptive vents active in historic time.

#### CRUSTAL STRUCTURE

Ryall and Bennett (1968), Hill (1969) and Eaton (personal communication, 1967) report seismic refraction data from explosions along the coasts of Hawaii and recordings both along the coasts and throughout the Island. All of these first-arrival data were combined on one travel-time versus distance graph, and an average travel-time curve was fit through the points. More weight was given to the south coast shot data because most seismic stations and earthquakes used in this study are near the south coast, because Ryall and Bennett (1968) suggest the presence of a great crustal thickness and possible deep faults between the north coast and Kilauea, and because Hill (1969) reports a large scatter in offshore travel times along the north coast. Parameters for two possible mean travel-time curves are given in Table 2, together with the crustal structures calculated from these curves. These two structures illustrate some of the latitude in fitting a model to the data. Structure A will be used in this study. Crustal structure (D) with a linear increase in velocity within the layers was derived by trial and error and is given in Table 2. This structure is not unique but does give travel times for *P* waves in the refraction experiments within 0.1 sec of structure A.

Structure C, derived by Eaton (personal communication, 1970) has been used for many of the routine locations reported by the staff of the Hawaiian Volcano Observatory. When crustal structures A and C are used, the computed epicenters are essentially the same, but for crustal structure A the depths are generally 1 to 2 km shallower, and the standard errors are lower.

There is as much as 1-sec scatter in the composite travel-time plot for observed travel times at constant distance. Generally, however, *P* waves from explosions detonated on the south coast arrive 0.18 sec earlier than the average travel time (structure A) at distances greater than 10 km. *P* waves from the north-coast explosions arrive generally 0.2 sec late at a distance of 10 to 30 km, as much as 0.8 sec late at 40 km, 0.4 sec late at 55 km, and 0.2 sec late at 60 to 100 km distance. It is clear from this wide scatter in travel

TABLE 2  
CRUSTAL STRUCTURES IN HAWAII\*

Model	Layer	Travel-time Intercept (sec)	P-Wave Velocity (km/sec)	Layer Thickness (km)
A.	1	0.0	1.8	0.2
	2	0.2	3.1	1.5
	3	1.0	5.1	3.7
	4	2.0	6.7	3.8
	5	2.6	7.4	4.0
	6	3.4	8.3	
B.	1	0.0	1.7	0.2
	2	0.2	3.3	1.6
	3	1.0	5.4	4.2
	4	2.0	6.7	6.2
	5	3.4	8.3	
C.	1		1.8	0.8
	2		3.1	1.4
	3		5.2	5.8
	4		6.8	5.5
	5		8.3	
	Layer	P-Wave Velocity at the Top of the Layer (km/sec)	Depth to the Top of the Layer (km)	Gradient in the Layer (sec <sup>-1</sup> )
D.	1	1.6	0.0	4.44
	2	2.4	0.2	2.07
	3	4.1	1.0	0.47
	4	6.0	5.0	0.23
	5	7.5	11.4	0.16
	6	8.3	16.5	0.01

\* Structures A, B and D are derived in this study. Structure C was derived by Eaton (Personal Communication, 1970).

times and the large variety of crustal structures reported by other workers in Hawaii that the mean crustal structure given here must be used with caution.

#### PRECISE HYPOCENTERS BASED ON *P*-WAVE ARRIVAL TIMES AT ALL STATIONS

More than 1,000 local earthquakes were recorded during the first 20 days of September 1967, when the array was operating most reliably. Many of these events were recorded by only some of the network and array stations, and many had unclear first arrivals. Therefore, the 43 largest events with clear *P*-wave arrivals (listed in Table 3) were chosen for careful study. *S* waves could be timed only to several tenths of a second and, thus, were not used in the hypocenter solutions. Hypocenters were determined using a computer program written by Lee (1970) and Lee and Lahr (1971) and based on an earlier program by Eaton (1969). Lee's program (1970) was considerably modified by the authors to run on an IBM 1130 computer. This hypocenter location program has two distinctive features:

travel times are calculated for each arrival from an assumed crustal structure (Eaton, 1969) and the hypocenter is calculated by Geiger's method (1912) using stepwise multiple regression (Lee, 1970; Draper and Smith, 1966). The hypocenter is calculated by minimizing the root-mean-square of the travel-time residuals (RMS in Table 3).

The most precise and accurate hypocenters should be those determined with data from the largest number of stations, provided the first arrivals at some stations are not inordinately biased by station elevation differences and lateral geological variations in crustal structure. The most precise hypocenters are considered in this paper to be those with the lowest rms and the smallest standard errors. Several types of station biases are examined below in an attempt to improve the precision and accuracy of the hypocenters calculated in this study.

*Elevation corrections.* Differences in station elevation constitute a special problem in the location procedure, particularly in Hawaii where station elevations vary by nearly 2 km. Stations at high elevations often have early arrivals and, in many cases, have high-velocity material at shallow depths beneath them. Normally, station elevation corrections are disregarded and, therefore, depths are calculated with reference to some poorly defined average station elevation.

For the purpose of this study, it was assumed as a first approximation that the main difference in crustal structure beneath stations at different elevations is in the crustal layer with a velocity of 5.1 km/sec (Table 2). Station C4 was chosen as the reference point and elevation corrections relative to C4 were calculated assuming as a first approximation that the wave travels vertically through this layer (Table 1). The 43 events were initially located using the elevation corrections.

*Station corrections.* Because large residuals at one or two stations usually cause mislocations of the earthquakes in this least-squares procedure, the largest residuals were examined carefully. *P* waves arriving at stations ML and MX from earthquakes to the southeast of the array (events 27 to 43, Table 3) and *P* waves arriving at MP and KX from earthquakes to the southwest of the array (events 8 to 21, Table 3) had widely scattered and large travel-time residuals no matter what elevation corrections or station corrections were tried. These arrivals were not used in the following analysis because they were emergent and because these waves probably travel through the most complicated structure in the volcano. Other miscellaneous arrivals were not used (labeled by B in Table 2) if they were unclear and gave large residuals. For example, the waves arriving at station N3 for events 4 and 5 were on a nodal plane defined by clear dilatations recorded at stations N1, N2, OT and clear compressions recorded at C4 and AH. The waves at N3 could not be directly correlated peak for peak with any of the waves at other array stations.

Beginning with the elevation corrections, several different attempts were made to find average constant station corrections. Residuals were found to be fairly consistent for earthquakes with hypocenters close to each other but different for earthquakes farther apart. Thus, three different sets of station corrections were calculated: for deep events, for events southwest of the array, and for events southeast of the array (Table 1). The resulting station corrections were subtracted from the arrival times and all events relocated with the result that the rms of the residuals were decreased by factors of from 2 to 6. These hypocentral locations and residuals are given in Table 3. There were only a few shallow events close to the array and they had widely varying residuals. Thus it was impossible to derive similar station corrections. Only altitude corrections were used for events 22 to 26.

The changes in hypocentral locations between the solutions using only altitude corrections and the solutions using station corrections which include altitude corrections

TABLE 3: LOCATIONS (LAT, LON, Z), STANDARD ERROR IN LOCATION (SELT, SELON, SEZ) IN KILOMETERS, ROOT-MEAN-SQUARE OF THE TRAVEL-TIME RESIDUALS (RMS), AND THE TRAVEL-TIME RESIDUALS IN HUNDRETHS OF SECONDS FOR THE EARTHQUAKES ANALYZED IN THIS STUDY. STATION CORRECTIONS IN TABLE 1 THAT INCLUDE ALTITUDE CORRECTIONS FOR  $v = 5.1$  KM/SEC WERE USED IN CALCULATING THESE HYPOCENTERS. DELAT, DLON, AND DZ ARE THE DIFFERENCES IN LATITUDE, LONGITUDE, AND DEPTH FOR THE HYPOCENTER DETERMINED WITH STATION CORRECTIONS MINUS THE HYPOCENTER DETERMINED WITH ONLY THE ALTITUDE CORRECTIONS FOR  $v = 5.1$  KM/SEC IN TABLE 1. LATITUDE AND LONGITUDE ARE GIVEN IN MINUTES NORTH AND WEST OF 19 DEGREES NORTH LATITUDE AND 155 DEGREES WEST LONGITUDE. ONE MINUTE EQUALS ABOUT 1.86 KM IN THIS AREA. ABOUT 1 KM SHOULD BE SUBTRACTED FROM THE DEPTH TO GET DEPTH RELATIVE TO SEA LEVEL. TIMES ARE IN DAYS, HOURS AND MINUTES FOR SEPTEMBER, 1967.

TIME (MIN)	LAT (MIN)	SELT (MIN)	LON (MIN)	SEZ (KM)	RMS (KM)	TRAVEL-TIME RESIDUALS IN HUNDRETHS OF SECONDS																										
						M1	M2	N3	E8	E9	E1	W5	W6	W7	C4	M4	AH	DE	NP	MP	KX	KV										
1	022142	23.3	0.2	-0.9	16.6	0.2	0.3	22.7	0.4	-1.0	1	1	1	-1	-2	2	0	0	1	0	0	1	0	1	0	3						
2	040610	23.5	0.1	-0.2	16.6	0.1	0.4	23.4	0.3	0.4	1	1	0	0	0	0	2	1	-2	0	-1	0	0	0	-1	1						
3	060215	22.9	0.2	-0.4	16.4	0.6	-1.4	27.2	1.6	0.8	1A	-2A	1	16E	1	2	0	-1	1	0	0	4	1	-1	-1A	1	0	-1				
4	071948	23.1	0.1	-0.3	18.0	0.1	0.3	22.2	0.3	0.3	1A	-2A	1	16E	1	2	0	-1	1	0	0	0	0	1	0	-1	1	0	-1			
5	081811	23.4	0.1	-0.3	17.5	0.1	0.3	19.7	0.2	0.2	1	0	2	2E	-1A	1A	0A	-2	1	0	1	1	0	0	1A	2	-1	1	-1			
6	061911	20.7	0.3	-0.2	17.8	0.3	0.2	24.2	0.7	-0.1	1	0	2	3	-2	-1	0	1	3	0	-1	3	-6	-5	-1	0	-1	0A	0			
7	080222	24.6	0.2	-0.3	17.4	0.2	0.2	14.8	0.3	0.1	2	4	1	2	1	2	3	-4	-2	-3	1A	1A	-4	-1	3	-1	1	0	-1	2		
8	021939	20.6	0.1	-0.2	19.5	0.1	0.1	3.5	0.1	0.1	1	X	X	X	0	2	-1	0	-2	-1	0	-1A	0A	1A	3	2	-1	-1	X	0A		
9	071955	20.6	0.1	-0.2	19.4	0.1	0.1	3.7	0.1	0.1	1	4	2	0	1	3A	-1A	-2	4	2	-1	-2	-1	-2	4	2	-1	-1	X	0		
10	071438	20.5	0.2	-0.2	19.5	0.2	0.0	4.0	0.3	1.0	5	0A	1A	3	1A	1	-3	-2	4	0	11A	-9	1	3A	1	2A	-5	X	X	-5A		
11	040024	20.2	0.2	-0.2	19.8	0.2	0.1	3.3	0.2	0.3	3	-3	-6	-7	-4A	0	2	1	4	2	2	-2	-1	-2	0	4	X	X	4			
12	130959	18.8	0.5	1.9	21.6	0.2	-0.9	3.8	0.3	-0.9	6	4A	-5C10	-3	-7	7	7	8	1	5	-4A	-3	3	-1	2A	5	-21B13B	2A				
13	101630	18.9	0.5	1.4	21.5	0.2	0.2	3.9	0.3	-0.8	5	8	4	1	-5	-9	-6	5	7	0	7	-4	-4	-3	-1	-6	0	-40B	3B	-2		
14	101632	18.7	0.5	1.6	21.5	0.2	-0.3	3.8	0.3	-0.9	5	9	5	1	-5	-8	-7	6	9	7	-3	5	-4	-5	-2	-1	-5	1	-81D	33B	-2	
15	061742	18.4	0.8	-1.2	22.9	0.4	0.6	4.4	0.2	0.9	5	1	-3	7	0	1	1	1	4	1	2	-1	6	10	3	-7	-6	-8	-5	5B	7B	-3
16	141750	17.4	0.8	-0.4	21.2	0.3	0.2	5.0	0.2	0.1	3	0	-1A	0A	1	2	0	1	1	2	-3	5	-1	-1	-1	-2	-9A	-7A	X	X	10A	
17	061153	18.1	0.6	0.6	22.9	0.3	-0.1	4.4	0.1	-0.1	2	-1	3	0	-2	1	-2	4	3	7	0	12	4	0	-2	-6	-8	-6	X	X	-4	
18	061930	19.2	0.5	-0.7	22.5	0.2	0.3	4.3	0.1	1.3	2	4	0A	-2	-3A	0	1	3	-2	2	1A	0	22B	3	4	1	-1	0	-11B	7B	1	
19	091308	17.9	1.6	0.2	27.2	1.1	2.2	23.9	1.9	5.7	4	-9	-6A	0	2	1	2	2	1	-2	-1	19B	1	-3	0	11	-1	-18	29B	5		
20	120127	20.5	0.6	-1.0	25.4	0.8	1.4	8.2	1.0	2.8	3	-3	-5	-6A	2	0	2	0A	-1	3	0	26B	2	0	0	-3	1	-13B	13B	7		
21	120138	21.5	0.4	-0.3	24.8	0.5	1.1	6.5	0.7	1.6	6	0	-3	-9	5	8	1	5	-9A	-8	-3	6A	X	-8	13	X	0	-3	X	X	1	
22	100754	24.0	0.2	0.0	16.9	0.2	0.0	1.5	0.1	0.0	9	-4	-9	-10	6	8	3	7	5	9	5	3A	X	-9	4	-14	-3	1	X	-13A	13	
23	190518	23.8	0.2	0.0	17.4	0.3	0.0	2.3	0.7	0.0	9	2	-7A	-9	4	3	3	7	6	5	1	14	4	-10	13	-15	1	-10	X	X	30B	
24	131718	24.5	0.2	0.0	17.9	0.3	0.0	0.1	1.4	0.0	5	-5	-4	-14B	1	0A	5A	6	1	2	6	-9A	-18	-8	3	-44B	-3	4	X	X	11	
25	032301	24.0	0.3	0.0	14.8	0.5	0.0	3.2	0.4	0.0	5	-1	-4	5	2	2	2	2	X	X	3	X	X	-2	-1A	X	22B	-7	X	X	17A	
26	070506	23.3	0.3	0.0	15.4	0.4	0.0	2.3	0.4	0.0	3	2	3	0	0	0	1	0	0	0	1	2	2	0	2	2	-2A	-1	1	-41B	9A	
27	060731	19.5	0.2	0.0	15.7	0.2	0.2	9.7	0.3	0.3	3	1	2	3	0	0	0	0	0	0	1	2	26B	X	0	2	-2	0	-4	-8	11A	0
28	080033	18.0	0.1	-0.1	15.4	0.1	0.1	11.8	0.2	0.6	2	3	2	4	0	-1	-2	-1	-1	1	0	-168	9B	1	0	0	-3	-2	0	-2	3A	1
29	060027	19.5	0.1	-0.1	14.0	0.1	0.1	10.1	0.2	0.3	2	-3	2	4	0	0	1	2	0	-1	0	208	6B	1	0	2	-1	0	-2	0	-3	3
30	032122	19.2	0.2	-0.1	13.6	0.1	0.0	10.7	0.2	0.5	2	-2	-2	0	0	1	1	1	1	1	X	X	X	-1	-1	-4A	X	X	1	0A	9A	
31	062140	19.3	0.2	0.0	13.6	0.1	0.0	9.7	0.3	0.9	2	1	0	2	-1	-3	-3	1	2	2	0	15B	4B	-1	-2	-2	-2A	-1	2	-1	-41B	
32	121950	19.6	0.1	-0.1	13.6	0.1	0.0	10.5	0.2	0.3	3	1	2	4	1	1	3	-3	-1	-1	1	39B	17B	-3	-5	3	4A	-7A	3	-2	2A	
33	071328	17.7	0.4	-0.2	12.5	0.3	0.0	13.5	0.5	0.6	2	4	2	0	-2	-2	2	3	1	2	2	26B	7B	-5	1	-3	-3	1	0	0	0	
34	030374	20.8	0.2	-0.1	12.9	0.2	0.0	11.4	0.3	0.6	2	3	-2	2	0A	-2	-3	2	1	1	2	28B	7B	1	6	-4	0	-1	-2	3	-1	
35	100535	21.5	0.2	0.0	13.8	0.1	0.1	10.7	0.3	0.8	3	4	1	3	-2	-1	-5	2	0	3	34B	21B	2	5	-3	-1	4	-1	-1	-13A		
36	101218	21.2	0.3	-0.1	11.1	0.4	-0.1	11.7	0.6	0.8	3	2	-4A	-4	1A	0	1	3A	-3A	3	15B	X	1	5	-6A	27B	-1	-3A	1	2A		
37	101219	20.9	0.3	-0.1	11.4	0.2	-0.1	10.5	0.5	0.8	4	3	-4	-4A	-4	-3	5	3	-9	2	0	32B	2B	3	7	1	-3	3	-4	2	-1A	
38	031705	19.3	0.5	-0.5	8.4	1.0	-0.7	12.3	1.1	1.8	5	1	-7	-8	-1	1	0A	0	-3	4	77B	3B	1	13	-10A	8A	3	0	0	-8A		
39	051610	20.9	0.6	-0.2	6.9	2.0	0.0	10.5	0.9	0.8	3	-1	-4	-4	0	0	1A	1A	3	-1	4	20B	X	2	2	-5	-8A	3	0	0	4	
40	072033	20.6	0.3	-0.2	6.6	1.3	0.4	10.5	0.9	0.8	7	-1	-4A	-1	6	4	4	9	-16	-11	8	61B	9B	3	7	-5A	-1	6	-10	3	4	
41	190241	21.9	0.8	0.0	6.7	2.0	1.3	9.2	0.5	2.4	4	-8	-1	-1	3	1	0	2	1	6	29B	X	0	2	-9	1	4	-2	0	1		
42	170419	22.0	0.4	0.0	6.3	0.8	0.0	8.9	0.2	0.1	4	-2	-2	-2	3	1	0A	2A	1	3	1	5	24B	X	2	-12	0	3	-4	1		
43	170439	21.9	0.4	0.2	6.2	0.9	1.6	8.9	0.2	1.9	4	-2	-2	-2	3	1	0A	2A	1	3	1	5	24B	X	2	-12	0	3	-4	1		

A = A QUESTIONABLE READING.  
 B = STATION ON THE NODAL PLANE NOT USED IN THE SOLUTION.  
 C = SAME AS A EXCEPT THE NEXT RESIDUAL IS NEGATIVE.  
 D = SAME AS B EXCEPT THE NEXT RESIDUAL IS NEGATIVE.  
 E = FIRST ARRIVAL COULD NOT BE READ.

are shown in Table 3; these changes are generally less than a kilometer in latitude, and depth. Calculating both station corrections and elevation corrections shows how much of the net station delay could be interpreted as related in some simple way to elevation differences and how much results from geological differences. The elevation corrections based on a velocity of 5.1 km/sec generally are a little closer to the final station corrections than those based on a velocity of 3.1 km/sec. Clearly from Table 1, however, the main travel-time corrections are caused by lateral variations in crustal velocities. These lateral variations are discussed in detail later in this paper.

*Distant P-wave arrivals.* All stations in Table 1 are within 30 km of the epicenters listed in Table 3. For several events, data from as much as six more stations, widely spaced over the Island, were available. These data generally had timing uncertainties of several tenths of a second. They were not used in the final solutions because the original records could not be read as accurately as the array or network records, because the use of separate clocks at these stations added a large additional timing uncertainty, because there is a wide scatter in travel times observed in the refraction studies at distances greater than 30 km, and because these data would have displaced the hypocenters in Table 3 by several kilometers and would have increased the residuals at the closer stations.

*Station location bias.* In order to evaluate whether a large number of stations at one azimuth or distance from the hypocenter would greatly affect the hypocentral solution, several hypocenters for a given earthquake were calculated using different subsets of the *P*-arrival data. Most solutions for different subsets of stations agreed with the solutions based on all of the data, although their standard errors were larger. Extreme examples are shown in Figure 2 where locations are plotted based only on network data, only on array data, and on all of the data. There is a slight tendency for an epicenter to be nearer to the array when all of the array data is used, but in these cases the inclusion of data from just one or two array stations has the same effect. Thus, the large number of array stations does not seem to significantly bias the hypocentral locations.

The large number of array stations does affect the calculated residuals, however, because the least-squares procedure is used in locating the earthquakes. If, for example, ML had a large negative residual and all of the array stations had no residual after one iteration in the derivation of a solution, the computer program would then cause all of the array stations to have small positive residuals and ML to have a less negative residual. This is another reason for selecting C4 as the reference station for altitude corrections. It is, also, the reason why some arrivals with obviously large residuals were not used, and why the relative level of the residuals is more important than the absolute level.

*Trial hypocenter.* For Geiger's (1912) method of hypocentral determination, a trial hypocenter is chosen and then corrected by iteration until the corrections become arbitrarily small or the solution is determined to fit adequately the arrival-time data. This method of successive approximations is necessary to linearize the equations. For a given trial hypocenter, successive approximations to the hypocenter will approach the minimum rms value by some route in hypocentral space (latitude, longitude, depth and time). For a different trial hypocenter, the approximations may approach the minimum along a different route. Depending on the termination criteria for iteration and on the curvature of the rms surface around the minimum, hypocenters calculated with the same data but from different starting points may differ by at least as much as the standard errors in latitude, longitude and depth.

In the use of stepwise multiple regression, one way of terminating the iteration is by the use of a "critical-*F*" value (Draper and Smith, 1966) that can be chosen on the basis of the number of arrival times and number of degrees of freedom. We found that, in order to avoid the effect of choice for trial hypocenters on the final solution, a critical *F*

value of about 0.5 was preferable to the statistically determined value of about 3. Several solutions were calculated for some earthquakes starting at a dozen different arbitrarily chosen trial hypocenters. In nearly all cases of events and trial hypocenters within or very near the network, the same final hypocenters were calculated. In one case where a trial hypocenter was about 10 km outside of the network, one solution was about 15 km from the other solutions and had a high rms value but appeared to be in a local minimum on the rms surface. In this study, the trial hypocenter was always chosen as being 5 km beneath the station with the earliest *P*-wave arrival time.

*Statistical evaluation of the precision of hypocenters.* The standard errors (Table 3) as commonly defined (e.g. Crow *et al.*, 1960) are measures of how well the arrival-time data fit the calculated solution and can be readily calculated in the hypocenter locating routine (Eaton, 1969). These errors are not necessarily a true measure of the precision of the hypocenters, however. The standard errors can sometimes be modified by more than a factor of 2 if only a few arrival times are changed within their expected error limits. If all travel-time residuals are subtracted from the observed arrival times and a new solution is calculated, then the standard errors become equal to zero. Thus, the standard error calculations used depend, in part, on the chance that the few data will have errors distributed symmetrically about the mean. Furthermore, this error estimate does not allow for input of statistics based on a large number of events or for input of independently derived error estimates of some of the variables used in calculating the hypocenters. The precision of the solution depends very much on errors in reading the arrival times. Other errors such as those in the location of the stations have significantly less effect in this study. Therefore, in order to estimate the hypocentral precision caused by timing errors alone, a random numbers approach was used where 100 solutions for several earthquakes were calculated. For each earthquake, the observed arrival times were randomly perturbed but in a manner such that the mean arrival time equaled the observed time and the standard deviation of the 100 arrival times at any one station equalled 0.01 sec for the array stations and 0.02 sec for the network stations. In other words, it was assumed that 95 per cent of the arrival-time data had absolute reading errors smaller than  $\pm 0.02$  and 0.04 sec.

Because, for a normal distribution, 95 per cent of the data should fall within 2 standard deviations of the mean, twice the resulting standard deviations in latitude, longitude, and depth are shown in Table 4. These values agree with the standard errors except that they are usually larger than the standard errors previously calculated. The standard deviations in Table 4 are the best measure of precision available for the events in this study. The precision is thus generally from  $\pm 0.1$  to 0.6 km in latitude,  $\pm 0.1$  to 2.3 km in longitude and  $\pm 0.2$  to 1.3 km in depth. If these precisions are used to plot the error limits in Figure 2, the different hypocentral solutions overlap each other more closely.

*Hypocenter accuracy.* The accuracy of the hypocenters is harder to evaluate than their precision. Systematic offsets in hypocenters have often been observed. Hamilton and Healy (1969), for example, found errors as large as 700 meters in epicenter and 400 meters in depth when locating a nuclear explosion, even though they had 27 seismographs operating within a circle 32 km in radius and centered about the explosion. Wesson (1971) found that the better located earthquakes at 1- to 4-km depth located with 13 stations within a radius of about 10 km may contain a systematic bias as large as 500 meters because of lateral variations in the seismic velocity. In both cases, seismic refraction data were available to give good data on the crustal structure.

Some considerations of accuracy can be seen in Figure 2. The epicenters and especially the calculated depth using array data only are poorly controlled when the epicenters are at distances of about the width of the array from the center of the array. Such solutions

TABLE 4: COMPARISON OF ERROR LIMITS FOR A FEW SAMPLE EARTHQUAKES. A IS THE STANDARD ERROR FROM TABLE 3. B AND C ARE TWICE THE STANDARD DEVIATION OF 100 SOLUTIONS. FOR B THE ASSUMED STANDARD DEVIATION OF THE P-WAVE ARRIVAL TIMES AT A GIVEN STATION IS 0.01 SEC FOR THE ARRAY AND 0.02 SEC FOR THE NETWORK. FOR C THE ASSUMED STANDARD DEVIATIONS ARE THE STANDARD DEVIATIONS OF THE RESIDUALS FOR EACH GROUP OF EVENTS IN TABLE 3.

EVENT	LATITUDE	LONGITUDE			DEPTH			AZIMUTH			
		A	B	C	A	B	C	A	B		
040610 DEEP	0.1	0.4	0.3	0.1	0.6	0.2	0.3	1.3	0.4	5	2
040024 SW	0.2	0.5	1.1	0.1	0.2	0.3	0.2	0.3	0.7	1	4
061742 SW	0.8	0.6	1.6	0.4	0.4	0.8	0.2	0.1	0.3	1	2
190518 NEAR	0.2	0.1	0.2	0.3	0.1	0.2	0.7	0.2	0.2	1	2
032301 NEAR	0.3	0.1	0.3	0.5	0.2	0.5	0.4	0.2	0.2	1	2
032122 SE	0.2	0.3	0.5	0.1	0.2	0.3	0.2	0.4	0.4	1	2
072033 SE	0.3	0.6	0.8	1.3	2.3	3.2	0.9	1.2	1.0	1	1

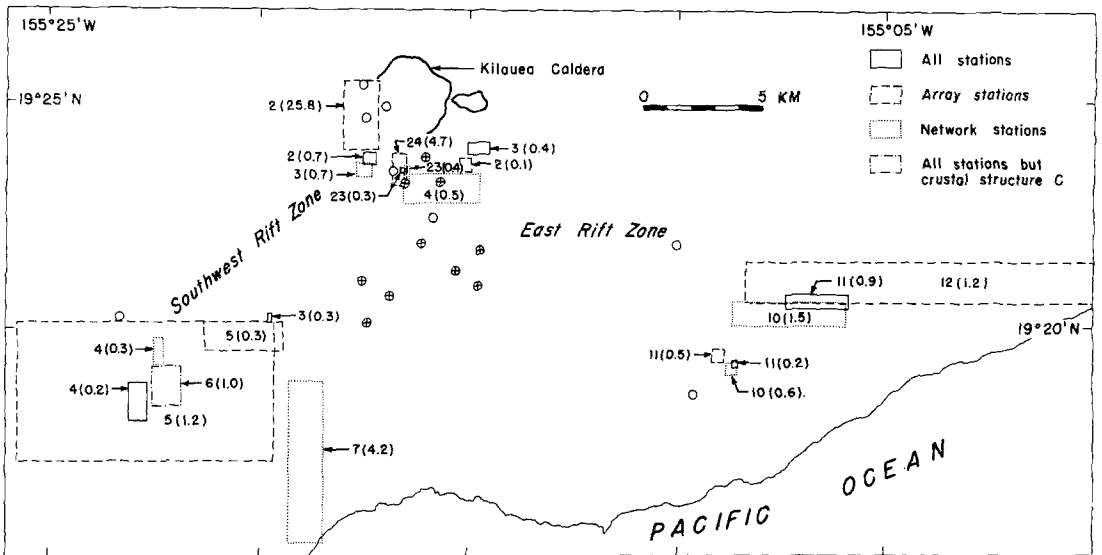


FIG. 2. Comparison of selected hypocenters located with different sets of data. The rectangles represent the standard errors in latitude and longitude. Numbers indicate depth to the nearest kilometer. The standard error in depth is given in parentheses.

do not necessarily have large standard errors in latitude, longitude or depth. For shallow events, it is more critical for a good solution to have a station near the epicenter. The depth calculated for an event tends to increase when data from the nearest station is not used. Thus, as might seem intuitively obvious, depths are most accurate when a station lies near the epicenter, and epicenters are most accurate when completely surrounded by seismic stations.

The accuracy is most affected by imperfect knowledge of crustal structure, which is crudely approximated by a layered structure (Table 2) and station corrections that vary with azimuth, distance and focal depth. One measure of the effect of station corrections is shown by the differences in locations based on different sets of station corrections (Table 3). Another possible measure is found by calculating standard deviation of residuals at each station for all of the earthquakes in Table 3 and assuming that the

resulting deviation for each station is a measure of the uncertainty in the choice of that station correction. These deviations are then applied in the random numbers analysis described above and standard deviations (Table 4) calculated for the coordinates of the selected events. This procedure suggests that the accuracies may vary from  $\pm 0.2$  to 1.6 km in latitude,  $\pm 0.2$  to 3.2 km in longitude, and  $\pm 0.2$  to 1.0 km in depth but larger inaccuracies cannot be ruled out.

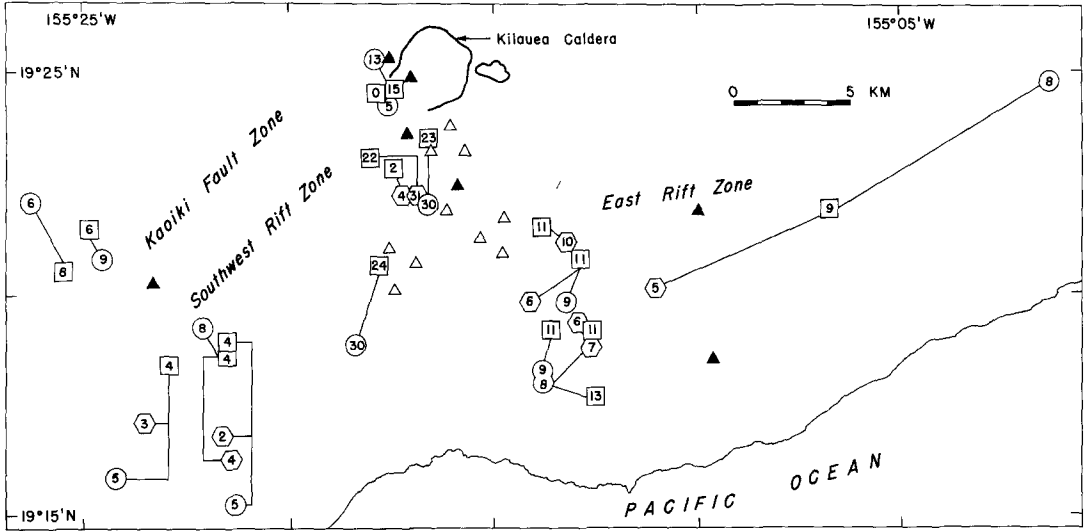


FIG. 3. Comparison of hypocenters located in this study (squares) with hypocenters reported by the staff of the Hawaiian Volcano Observatory (Okamura *et al.*, 1969) (circles) and computer locations without station corrections similar to those reported by the Observatory staff for 1968 through 1971 (hexagons). Open triangles represent the array, and solid triangles, the network stations, respectively. Numbers represent depths and error on depths as in Figure 2.

*Comparison with locations reported by the Hawaiian Volcano Observatory.* The locations listed in Table 3 are the most precisely and accurately located earthquakes yet available on Kilauea Volcano and, thus, can be used to evaluate the accuracy of the routine locations of earthquakes published by the Hawaiian Volcano Observatory. Figure 3 shows a comparison of the events in this study that were also reported by Okamura *et al.* (1969). Their locations were determined by use of isochrons (Nersesov and Rautian, 1960). Computer-determined locations based on the same data as the isochrons are also given. These computer locations were determined in a manner similar to that used for events reported from 1968 through 1971 (Endo, personal communication, 1972). Differences of 5 km in these various locations of the same events are common and a difference of about 15 km was observed. Thus, the locations reported so far in the Hawaiian Volcano Observatory summaries should be used with care for drawing detailed conclusions relating earthquake hypocenters to geological features. Since the most accurate, routinely reported hypocenters on any volcano in the world are those from Hawaii, this study emphasizes that the detailed relation of shallow earthquakes to volcanoes is still very poorly known.

#### LOCATION OF LOCAL EARTHQUAKES USING DATA FROM TRIPARTITE ARRAYS

Data from a single tripartite array allow computation of the azimuth of approach and apparent velocity of incoming seismic waves. Locations of local earthquake foci can be calculated by tracing a ray with the computed apparent velocity through an assumed

crustal structure to the earthquake hypocenter. The length of the ray is defined by the  $S-P$  time. The geometry of the array and the assumed crustal structure strongly influence the precision of the locations of events whose epicenters are outside the array. Shallow earthquakes whose first arrivals are critically refracted waves, or head waves, cannot be located uniquely if a crustal structure with layers of constant velocity is assumed. If the discontinuities in the velocity distribution are eliminated by assuming a structure with velocity that increases continuously with depth, then shallow earthquakes can be located uniquely, although not necessarily accurately, and the errors in location caused by uncertainties in reading the first-arrival times become a smooth function of these timing uncertainties.

Problems with the usual methods for calculating errors and the treatment of refracted waves are outlined in the appendix together with a method of determining errors resulting from errors in reading the  $P$ -wave arrival times.

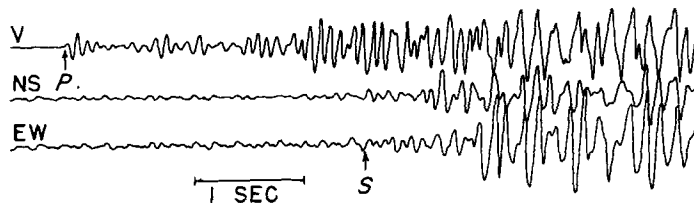


FIG. 4. Three-component recording of a deep event (071948) at station C4. The predicted arrival of the  $P$  and  $S$  waves shown are based on the location in Table 3.

*Accuracy and precision of array locations in Hawaii.*  $S$  waves observed in this study generally were emergent and slowly increased in amplitude over an interval of 1 to 2 sec (Figure 4). Thus, it was usually not possible to pick the arrival of  $S$  to better than at least several tenths of a second. Some other phase could often be mistaken for  $S$  on the horizontal seismometers and was usually mistaken for  $S$  on the vertical seismometer (Figure 4). The lack of clear  $S$  phases severely limits the usefulness of tripartite arrays in Hawaii and many other areas. Only azimuths from the arrays to the hypocenters and apparent velocities will be discussed in detail here.

The 10 array stations were combined into seven different tripartite arrays of varying size and geometry. Azimuths to sample earthquakes from the centroid of each of these arrays are shown in Figure 5 together with the precisions as defined in the appendix. The error limits are calculated assuming an error of 0.01 sec in reading the arrival times. Azimuths and apparent velocities and their precisions are given in Table 5 for the north (N1, N2, N3), east (E8, E9, E1), and west (W5, W6, W7) arrays and compared with the predicted values assuming the hypocenters given in Table 3. The predicted azimuths are assumed to have errors of a few degrees resulting from uncertainties in the earthquake locations (Table 4), if the assumed error in reading arrival times is increased slightly, and if data for the deep events and a poorly located close event (event 26) are ignored because of the large uncertainties in the predicted azimuths, then only 11 per cent of the observed azimuths are significantly in error (asterisks in Table 5) and one half of these are based on at least one slightly unclear reading of the  $P$ -wave arrival time. Roughly, the same percentage of apparent velocities agree although the problems in assuming a crustal structure adds a considerable uncertainty to the predicted apparent velocities. In most cases, the calculated azimuths and apparent velocities agree with the values expected from the hypocenters listed in Table 3. The azimuths to deep earthquakes directly below the array are very unreliable. Differences of as much as  $41^\circ$  between predicted and observed

azimuths for events to the southwest and southeast of the array show that large inaccuracies in hypocentral location can occur when data from only one tripartite array are used. Naturally, the hypocenters determined with data from one tripartite array have larger uncertainties in location than those determined with data from up to 20 stations. These uncertainties are large enough that evidence for lateral refraction of *P* waves in the crust would be quite ambiguous if based only on the deviations in azimuth.

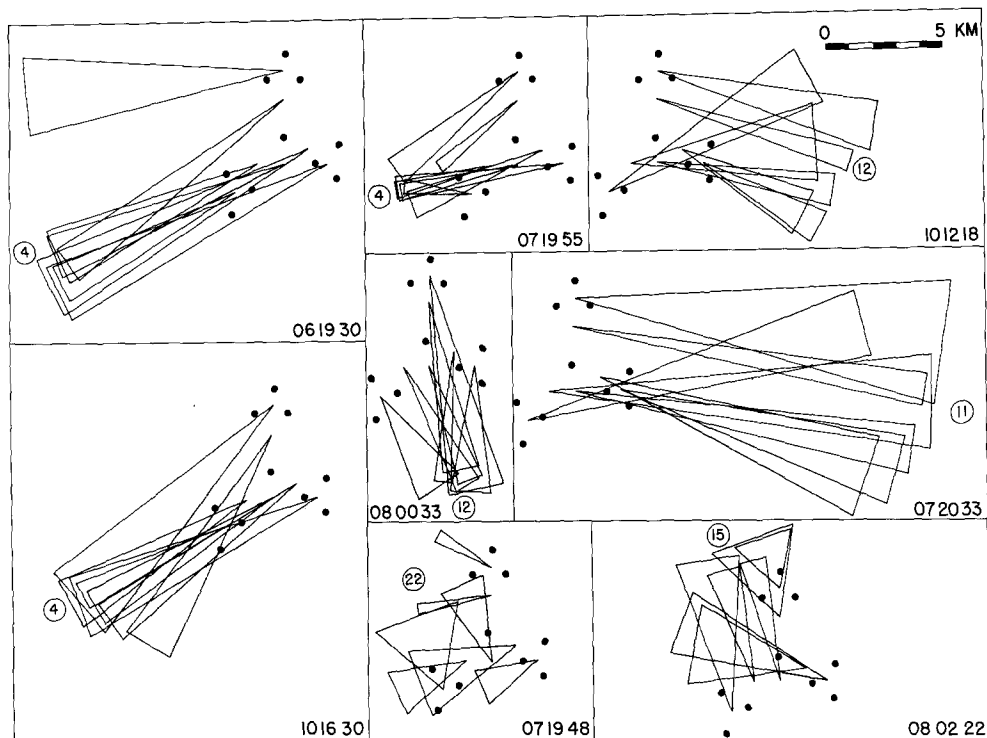


FIG. 5. Azimuths observed at several different tripartite arrays for a few typical earthquakes. The observed azimuth plus and minus the error expected from an 0.01-sec error in reading the arrival times is shown by the two long sides of the triangle. Each triangle originates at the centroid of the three stations used in the calculation.

#### EVIDENCE FOR REGIONS OF ABNORMALLY HIGH AND LOW VELOCITY NEAR KILAUEA VOLCANO

The travel-time residuals and differences in predicted and observed azimuths of *P* waves approaching the arrays discussed above, together with refraction data and geological observations discussed below combine to give detailed, but somewhat ambiguous, evidence that the crust under the rift zones and Kilauea Crater has slightly higher than normal seismic-wave velocities, and that the crust under the Kaoiki fault zone and possibly the region just south of Kilauea Crater have slightly lower than average velocities. These data will now be summarized.

Examining differences between predicted and observed azimuths and apparent velocities is simply another way of visualizing the meaning of the travel-time residuals. If the residuals are subtracted from the arrival-time data, the predicted and recalculated azimuths and apparent velocities agree. The residuals can be interpreted more directly, are quite consistent for many earthquakes, and are significantly larger than the assumed 95 per cent confidence limits of the reading errors (0.02 to 0.04 sec).

*Travel-time residuals.* Geologically, the most interesting travel-time residual for a

TABLE 5: AZIMUTHS, APPARENT VELOCITIES, AND THEIR ERRORS ASSUMING A TIMING ERROR OF 0.01 SEC FOR THE NORTH, EAST, AND WEST ARRAYS. P-0 IS THE PREDICTED VALUE BASED ON THE LOCATIONS IN TABLE 3 MINUS THE OBSERVED VALUE. TIME IS IN DAYS, HOURS, AND MINUTES FOR SEPTEMBER, 1967.

TIME	AZIMUTHS (DEGREES)									APPARENT VELOCITIES (KM/SEC)									
	NORTH ARRAY			EAST ARRAY			WEST ARRAY			NORTH ARRAY			EAST ARRAY			WEST ARRAY			
	DYHRMN	OBS	ER	P-0	OBS	ER	P-0	OBS	ER	P-0	OBS	ER	P-0	OBS	ER	P-0	OBS	ER	P-0
<b>DEEP EARTHQUAKES</b>																			
1	022142	143	54	X	234	29	91	340	20	38	L.	L.	X.	28.1	12.1	9.6	19.2	5.8	10.4
2	040610	145	89	X	248	24	76	350	22	22	L.	L.	X.	24.1	11.8	10.5	19.8	4.8	9.8
3	060215	X	X	X	X	X	X	328	38	52	X.	X.	X.	X.	X.	X.	38.6	30.6	5.0
4	071948	301A	6-40		246	17	55	340	30	4	5.8A	0.9	43.0	16.7	5.5	8.5	28.3	12.6	6.3
5	081811	309A	4	L	263A	14	48	352	23	4	4.4A	0.5	47.6	15.6A	6.4	28.0	21.5	5.5	6.3
6	061911	218	24	-6	242	15	15	326	29	L	21.8	7.7	7.7	13.4	3.2	21.2	29.2	18.0	L.
7	080222	342	30-26		291	11	34	352	13	6	3.8	24.9	-5.2	12.9	3.3	1.2	11.5	1.6	2.6
<b>EARTHQUAKES TO THE SOUTHWEST OF THE ARRAY</b>																			
8	021939	X	X	X	252	4	9	272	5	-2	X.	X.	X.	4.6	0.5	0.7	7.3	1.3	-1.3
9	071955	233	6	-4	263A	4	-2	278	6	-8	5.3	0.5	0.0	4.4A	0.5	0.9	7.5	1.2	-1.2
10	071438	220A	5	8	252A	5	7	273	7	-7	4.7A	0.3	0.7	5.3A	0.6	0.1	9.1	1.9	-2.6
11	040024	232	7	-4	261	4	-4	252	5	9	7.0	0.9	-1.8	4.1	0.4	1.1	6.6	1.1	-0.9
12	130959	206A	11	22	244	6	4	239	6	7	10.5A	2.2	-5.3	5.6	3.6	-0.3	7.1	1.0	-1.8
13	101630	226	8	2	248	5	1	244	6	2	7.8	1.0	-2.5	5.5	3.6	-0.2	7.8	1.3	-2.4
14	101632	218	8	10	248	5	-1	241	6	4	7.7	0.9	-2.5	5.4	0.6	-0.2	7.6	1.2	-2.3
15	061742	274	8-41*		249	5	0	247	7	1	6.4	0.7	0.3R	5.4	0.6	-1.3R	8.2	1.5	-2.9
16	141750	227	7	-8	245	6	-8	232	8	-3	6.3	0.7	0.4R	5.9	0.7	0.8R	8.7	1.3	M.
17	061153	241A	8-10		242	6	5	238	6	7	8.1A	1.5	-1.4	5.8	0.6	0.9	7.0	1.0	-1.7
18	061930	265A	8-30*		245A	6	9	244	6	10	6.8A	0.7	M.	5.5A	0.6	1.2	6.7	1.0	-1.4
19	091308	242A	17	1	259	6	-5	259	7	3	11.2A	2.9	-0.4	7.0	1.2	3.6	10.0	2.8	2.0
20	120127	272A	6-20*		262	6	3	278	6	-9	5.1A	0.4	1.8	6.4	1.1	0.4	7.2	1.1	-0.2
21	120138	266	10-11		262	6	7	281A	6	-7	8.2	1.0	-1.4	6.7	1.2	0.1	7.3	1.1	-0.5
<b>EARTHQUAKES NEAR THE ARRAY</b>																			
22	100754	302	7	7	316	6	10	326A	5	3	7.3	1.5	-3.4	7.1	1.1	-2.0	5.0A	0.5	0.1
23	190518	291	8	-3	308	6	9	357	7	1	7.8	1.4	-4.4	6.6	0.8	-3.4	6.1	0.5	-2.9
24	131718	315A	3-11		318	5	1	343	5	7	3.9A	0.3	-0.8	5.9	0.8	-0.8	5.0	0.4	0.1
25	032301	90A	6-25		359A	5	4	29	6	-4	5.3A	0.4	1.6	4.8A	0.4	0.7	6.3	0.7	-1.0
26	070506	51	12	39	3	6-17	X	X	X		11.1	2.3	-3.3	5.8	0.5	-0.6	X.	X.	X.
<b>EARTHQUAKES TO THE SOUTHEAST OF THE ARRAY</b>																			
27	060731	163	7	11	186	12	15	130	11	-4	7.4	1.2	2.1	10.6	1.7	5.2	13.4	3.4	3.1
28	080033	168	8	5	183A	10	5	147	13	-1	8.9	1.9	0.5	8.6A	1.0	4.0	12.9	3.4	0.3
29	060027	148	8	5	155	10	-1	103	7	7	9.3	1.6	0.0	9.8	2.4	6.0	9.1	1.6	2.0
30	032122	151	8	0	160	12-10	100	8	13		8.4	1.3	0.9	11.7	3.0	2.6	10.8	2.4	-0.1
31	062140	147	8	4	150	9	-2	99	7	12	8.9	1.5	-0.3	9.8	2.5	3.4	8.8	1.6	1.1
32	121950	142	8	7	140	8	5	98	7	9	9.3	1.8	0.2	9.7	2.1	6.1	9.5	1.9	1.4
33	071328	163	9-15		155	11	-8	107	8	15	10.1	2.3	-1.6	11.3	3.1	-0.4	9.6	1.7	-0.2
34	030324	121	7	10	135	12-29*		73	8	15	7.3	1.5	3.6	13.3	3.8	7.3	10.1	2.5	0.6
35	100535	111	9	20*	118A	13-36*		65	7	10	8.0	1.5	4.6	14.9A	4.0	13.7	8.9	1.8	2.3
36	101218	110	7	16*	112	8-29*		75	7	10	6.2	0.9	3.3	9.2	1.4	2.8	9.1	2.2	0.2
37	101219	104A	7	16*	119A	7-22*		61A	7	26	6.6A	0.9	2.3	8.3A	1.2	3.3	8.5A	1.5	0.1
38	031705	106A	6	13	101	15	7	129	7-30*		5.7A	0.7	2.5	17.5	7.2	-8.6	9.2	1.6	-1.0
39	051610	98	6	8	107	7-14		75A	6	13*	5.0	0.4	2.6	8.5	1.5	-0.7	7.7A	1.6	-0.1
40	072033	99	7	10	106	7-11		75A	5	15*	6.0	0.7	1.6	7.9	1.3	-0.2	7.3A	1.4	0.3
41	190241	93A	8	7	95	5-9		X	X	X	6.8A	0.7	0.6	6.7	1.1	M.	14.6	5.1	-7.2
42	170419	120	8-21*		98	5-13*		73	5	10	7.9	1.7	-0.9	6.7	1.1	0.4	6.1	0.9	1.3
43	170439	106	6-7		90A	6-4		73	5	10	5.8	0.7	1.2	7.0A	1.4	0.1	6.6	1.1	1.7

A= QUESTIONABLE READING IS USED.

L= P-0 IS GREATER THAN 99.

M= DIRECT WAVE TO ONE STATION AND REFRACTED WAVE TO ANOTHER STATION.

R= REFRACTED ARRIVALS AT ALL THREE STATIONS.

\*= THE OBSERVED AND PREDICTED AZIMUTHS ARE SIGNIFICANTLY DIFFERENT.

station and one earthquake is the observed travel-time residual (Table 3) plus the station correction and minus either of the elevation corrections (Table 1). The travel-time residuals for the deep earthquakes are so small (Table 3) that they probably result primarily from timing errors. The station corrections (Table 1) which were used in locating all of the earthquakes in Table 3, thus fairly reliably show that stations on the rift zones and near Halemaumau (DE, NP, WP, HV, MP) receive P waves 0.1 to 0.15 sec earlier than expected for their elevations. Arrivals at MX are late by more than 0.1 sec. Because the main criterion for calculating a hypocenter is to find a least-squares fit to the arrival time which minimizes the station residuals, it is not possible to determine the absolute level of these residuals from only arrival-time data for a few earthquakes.

P waves from events along the southwest rift arrive earlier than expected at station N2

and later than expected at N1. The observed azimuths are thus from the west-northwest rather than the southwest for events 15, 16, 17, 18, 20 and 21. Arrivals for event 12 were poorly recorded at the north array and thus the calculated azimuth from the north array is probably in error. *P* waves from all the southwestern events arrive about 0.1 sec early at the summit stations (NP, WP), slightly early at AH, OT, HV, N1 and N2, generally 0.1 to 0.15 sec late at MX, and slightly later at W6 and W7. Note that *P* waves traveling along the Kaoiki fault zone from events 19, 20 and 21 to station MX arrive more than 0.3 sec late.

*P*-waves from events to the southeast generally arrive from a more northerly direction than predicted at the north and west arrays and more southerly direction at the east array. This feature shows up in the residuals (Tables 1 and 3). Arrivals at W6 are later than expected and arrivals at N2 are earlier than arrivals at N1 or N3. One interpretation of these data is that the waves travel more rapidly along the east rift zone and the Koaie fault zone than along the direct path. Another possibility suggested by the positive residuals at N1, N2, N3 and OT is that the crust under these four stations has slightly lower than normal velocities.

Too few data are available for earthquakes near the array to make many generalizations. Note, however, that the residuals are usually positive at E8, E9, E1, W5, W6, W7, and OT but negative at stations AH, N1, N2, N3, WP, and NP, which are usually the closest stations. These arrivals again suggest that the uppermost crust near OT has slightly lower than normal velocities and that waves traveling through the crust to a depth of a few kilometers under the array and particularly under the Koaie fault zone arrive slightly later than normal. Late arrivals are early at DE, which is consistent with observations of events to the southwest of the array.

*Refraction data.* Travel times from explosions along the coast of Hawaii (Hill, 1969) to stations ML, AH, DE, WP, and MP were re-examined and compared with structure A in Table 2. The observed travel times minus those predicted from the crustal structure (in tenths of a second) are plotted in Figure 6 at the end of a line pointing from a given station to the shotpoint. As in the derivation of structure A, no correction was made for station elevation, but corrections were made for the height of the shot above the ocean floor. The distances are from 12 to 101 km and the rays probably travel to depths of from 3.5 to 17 km, whereas the refracted rays from the earthquakes in Table 3 travel no more than 30 km in horizontal distance and only to depths of about 6.5 km. Thus, these two data sets are not strictly comparable. For the shorter paths in Figure 6, waves traveling nearly along the rift zones generally arrive 0.1 to 0.3 sec early, whereas waves traveling to AH from the southeast or southwest generally arrive 0.3 sec late. An unpublished analysis of these data by Hill (personal communication, 1967) also suggests that the crust under the rift zones has higher than average velocities. Corrections for station elevation would tend to reduce the residuals in Figure 6 by approximately 0.1 sec or, in other words, would make the apparent rift zone velocities higher but would not change the relative residuals at a given station.

*Related observations.* Increasing evidence from geological mapping, tilt measurements, leveling and geodimeter data suggest that the rift zones on Kilauea are dilating and being intruded by dikes (Moore and Krivoy, 1964; Fiske, 1969; Swanson *et al.*, 1971). These systems of dikes most likely have slightly higher velocities than the thick sequences of lava flows making up the volcano, because the dikes are massive whereas the flows are jointed, interbedded with clastics, and filled with both lava tubes and flow rubble. A center of ground inflation (Fiske, 1969) believed to be caused by a magma reservoir at a depth of a few kilometers (Eaton, 1962) or only 1 km (Dieterich, 1972) is often observed in the region of stations AH, OT, N1, N2, and N3.

*Interpretation of the travel-time residuals:* The magnitude of the travel-time residuals observed in this study is generally  $\pm 0.1$  to 0.2 sec or about  $\pm 3$  to 6 per cent of most travel times. These results suggest that the average velocities vary along the whole path by  $\pm 3$  to 6 per cent, that they vary significantly more in a small region, or that the velocities vary by  $\pm 5$  to 10 per cent over the whole path if lateral refraction occurs causing longer travel paths. Another explanation of the variations in travel time is that velocities are always as shown in model A (Table 1) but the layers are of variable thickness. For a wave traveling vertically, a negative residual of 0.1 sec could be explained, for example, by assuming that layer 3 of model A in Table 2 ( $V_p = 5.1$ ) is 2.1 km thinner and layer 4 ( $V_p = 6.7$ ) is 2.1 km thicker.

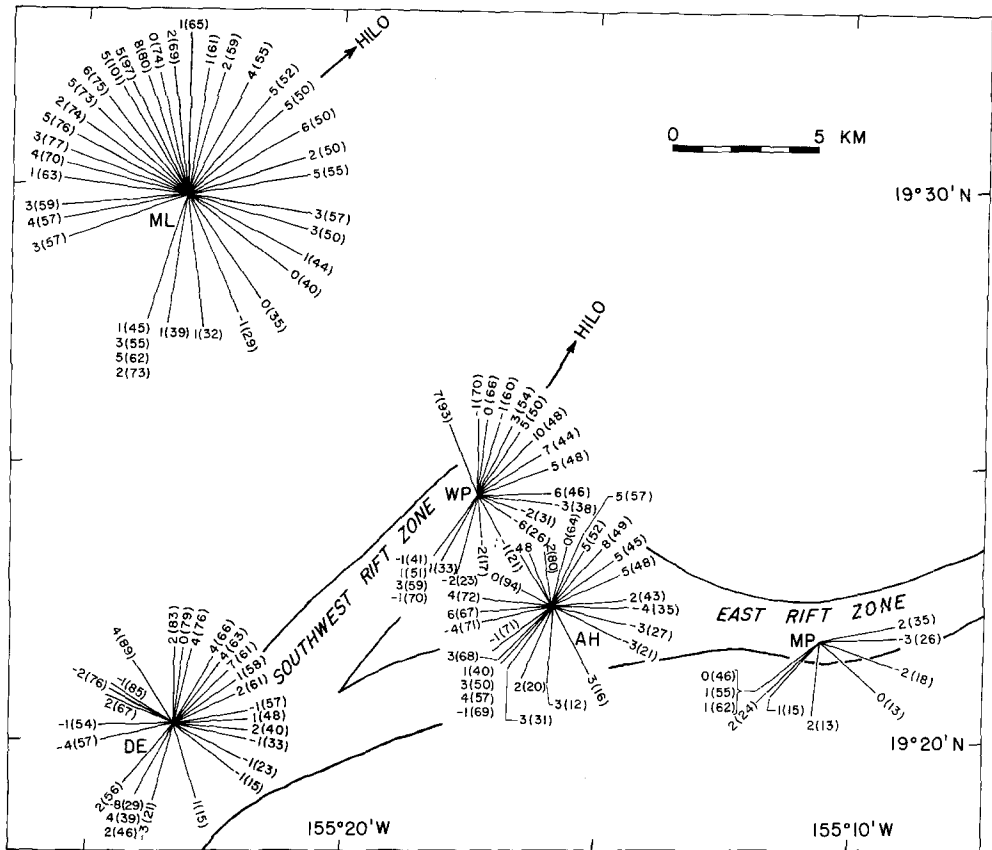


FIG. 6. Summary of travel-time residuals for the refraction data reported by Hill (1969). The observed travel time minus the time predicted from crustal structure A (Table 2) is shown at the end of a line originating at the stations (and pointing toward the shotpoints). The units are tenths of a second. The station to shotpoint distance (in kilometers) is shown in parentheses. Station MP was moved slightly between the time of the refraction experiment and this study.

The clearest and most easily interpretable residuals are those for the deep earthquakes. Stations on the rift zones receive waves 3 to 5 per cent faster than the other stations. The percentage is calculated by comparing the observed and calculated travel times. Assuming this travel-time anomaly is caused by intrusion of dikes into the upper 5 km of the crust where the velocities have been assumed to be less than 6.7 km/sec, then the velocity of the upper crust would need to be about 10 per cent higher than normal. Basalts typically have velocities of the order of 4.5 to 5.5 km/sec whereas diabase dykes typically have velocities of about 6 to 6.5 km/sec (Anderson and Liebermann, 1966; Manghni and Woollard, 1968). Thus, the travel-time anomalies for the deep earth-

quakes can be adequately but not uniquely explained by a mixture of layered basalts cut by dikes in the rift zones. Crustal model A (Table 2) was intentionally chosen to fit the average travel times in the Kilauea region. As shown by the positive residuals at most azimuths in Figure 6, however, an average crustal structure over the whole Island would give greater travel times. Thus, the anomalies observed in the rift zones would be larger than those given here if they were compared with the average crustal structure away from a volcanic center. This difference might be attributed to dikes scattered throughout the volcanic pile but more likely is caused by a thicker pile of lava flows and sediments away from the main volcanic vents and a thinner crust under these vents (Hill, 1969).

The apparent refraction of waves along the rift zones from events to the southwest and southeast of the array also can be adequately explained by the presence of many dikes under the rift zones.

The positive residuals at MX seem best explained by the rocks in the Kaoiki fault zone having lower than average velocities. Waves from most earthquakes arrive about 0.1 sec later than expected. Although this difference could be explained by a small zone of abnormally low velocity beneath the station, waves that travel directly along the Kaoiki fault zone (events 19, 20, 21) arrive 0.3 sec late. This anomaly implies that the average velocity along the path is about 10 per cent slower than in the model. Such differences might be explained by intense fracturing or an abnormally thick layer of low-velocity materials. If the region of low velocity was very wide in an east-west direction, its effect should be noticeable on the arrivals at ML. The Kaoiki fault zone divides Kilauea Volcano from Mauna Loa Volcano and is a region of fairly continuous seismic activity (Koyanagi *et al.*, 1966).

The station corrections for deep earthquakes suggest that velocities along the Koaie fault zone may be slightly slower than normal. Travel-time residuals for the events to the southeast of the array, however, could be interpreted to say that waves travel faster along the Koaie Fault zone than they do south of it. One or more of the layer interfaces could be sloping down in a southerly direction under the Koaie fault zone. Any high or low velocity anomaly here is certainly not as large as that on the east and southwest rift zones. This conclusion fits with the geological observations that the Koaie fault zone consists primarily of cracks and normal faults with less evidence of dike intrusion and eruption than along most parts of the rift zones (Moore and Krivoy, 1964; Walker, 1969).

Some evidence was given above for the crust under stations N1, N2, N3, OT and AH having slightly lower than average velocities. These anomalies are of particular interest because other data (e.g. Eaton, 1962; Dieterich, 1972) suggest the presence of a magma chamber at shallow depth in this region. The seismic data in this region are unfortunately too few and ambiguous to delineate clearly the anomalies. Certainly the  $P$ -wave velocities in this region are lower than those in the rift zones but they may not be much lower than average. No obvious attenuation of  $S$  waves was observed similar to that reported by Gorshkov (1971), Matumoto (1971) and others even for wave paths that passed through the supposed magma chambers.

#### FOCAL MECHANISMS

Focal mechanism solutions were attempted for all 43 events in Table 3. For one event, all dilatations covering a large part of the focal sphere were recorded (Figure 7a). When the depth to this shallow event was changed from 0.3 to 0.1 km, substantially less than the standard error, all points moved toward the center, where they fit a normal faulting type double-couple solution (Figure 7b). This dramatic change occurs because one of the layer boundaries in the crustal structure is at 0.2 km depth. This example clearly illustrates

some problems in determining focal mechanism of shallow events especially in a layered crustal structure and supports the suggestion by Zobin (1970) that single polarity events reported near volcanoes on the basis of few data by Minakami (1960), Minakami (1964) and Wada and Sudo (1967), for example, might well fit double-couple sources if more data were available.

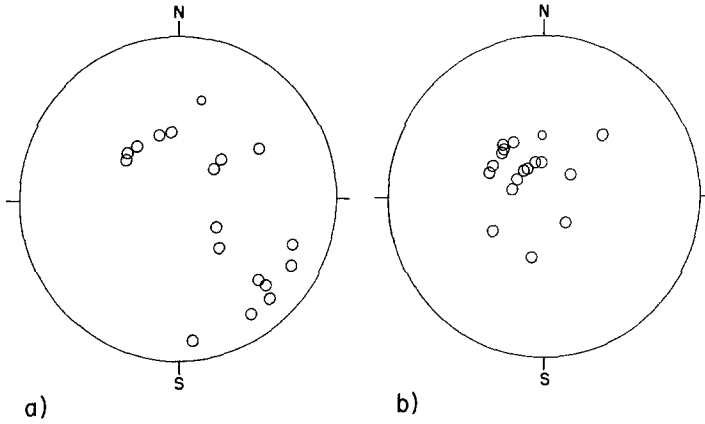


FIG. 7. Plots on the lower focal sphere of dilatational first motions observed for event 24 assuming a focal depth of 0.1 km (a) and 0.3 km (b).

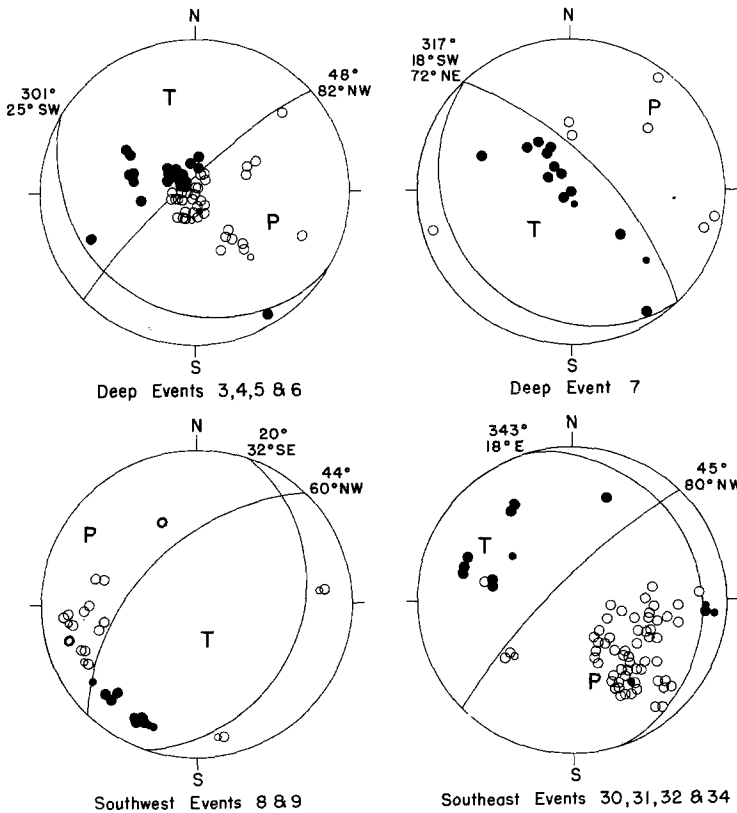


FIG. 8. Plots on the lower focal sphere of first motions for three different groups of earthquakes and one separate earthquake. Open circles represent dilatation and closed circles represent compression. *P* and *T* are the inferred axes of maximum and minimum stresses, respectively. The numbers are the strike and dip of the nodal planes.

Many of the other events that grouped spatially had very nearly the same focal mechanism. Composite first motion plots for these groups and the implied axes of maximum ( $P$ ) and least ( $T$ ) stress are shown in Figure 8.

#### CONCLUSIONS

The locations of 43 earthquakes on Kilauea Volcano in Hawaii have been carefully determined with data from a network of ten stations distributed throughout the region and an array of ten stations located in a small area and arranged to form several small tripartite arrays. A new average crustal-structure was derived by compiling all available refraction data. Travel-time residuals, with regard to this structure, of up to a few tenths of a second were observed. Waves traveling along the east and southwest rift zones of Kilauea Volcano arrive earlier than average. This anomaly can be explained, although not uniquely, by dikes which intruded into the rift zones. Waves traveling along the Kaoiki fault zone arrive late apparently because of intense fracturing or a rapid change in crustal structure. Some evidence suggests that the region just south of Kilauea Caldera may have slightly lower than average velocities.

The errors in earthquake locations determined with data from a tripartite array may change significantly with azimuth from the array and for different array geometry. For an array with sides 1 to 2 km long, the most accurate and precise locations are for events within 5 to 10 km from the center of the array. Less scatter in hypocenters and unique locations for shallow earthquakes whose first arrivals are refracted waves can be obtained if a crustal structure with layers of linear increase in velocity is assumed rather than a structure with several layers of constant velocity.

Because  $S$  waves could not be read clearly in this study, only azimuths and apparent velocities of waves approaching the tripartite arrays could be analyzed and compared to the values predicted from the hypocenters determined using  $P$ -wave arrivals at up to 20 stations. Generally the observed and predicted azimuths and apparent velocities were the same within their observational errors. A tripartite array could in this case be used reliably to locate roughly many local earthquakes. Some observed azimuths and apparent velocities, however, differed by more than  $40^\circ$  and a factor of 0.4 to 1.7, respectively, from the value predicted from the hypocenters located with all available data. These deviations can be explained by very small changes in crustal velocities or thicknesses. Thus, tripartite arrays may give totally erroneous locations in some situations and extreme care must be taken in calibrating the array locations and interpreting the data. Because of the problem of observing and accurately timing  $S$  waves, an array with four or more vertical geophones would be far more useful than a tripartite array for locating local earthquakes. Examining travel-time residuals at a number of widely separated stations proved in this case to be a more accurate way of studying lateral refraction in the crust than examining deviations in azimuths recorded at a number of tripartite arrays.

#### ACKNOWLEDGMENTS

Elliot Endo prepared the array equipment for the field and carried out a major part of the field installation, maintenance, and surveying. His skill and energetic assistance are largely responsible for the success of the field work. The staff of the Hawaiian Volcano Observatory of the U.S. Geological Survey assisted this project in many ways. In particular, Dick Fiske did much of the surveying of the array, George Kojima aided in installation and repair of the array and timing system, and Bob Koyanagi provided advice and data from the network of seismometers operated by the observatory. Jerry Eaton provided the impetus to start this project, assisted in part of the field work, and made many valuable comments during the data analysis. Dave Hill and Alan Ryall provided their original refraction data. Several dis-

cussions with Keith McCamy proved valuable. Sveinbjörn Björnsson assisted in some derivations of equations in the appendix. This manuscript was critically reviewed by Robert Hamilton, David Hill, and Jerry Eaton of the USGS National Center for Earthquake Research, Bob Koyanagi and John Unger from the USGS Hawaiian Volcano Observatory, Christopher Scholz and Paul Richards of Lamont-Doherty Geological Observatory, and Sandra Ward. We greatly appreciate all this assistance.

Much of this work was done while both authors were at Lamont-Doherty Geological Observatory under Contract 14-08-0001-11182 with the U.S. Geological Survey. The research was partially supported by the Advanced Research Projects Agency of the Department of Defense and was monitored by the Air Force Cambridge Research Laboratories under Contract F 19628-71-C-0245.

APPENDIX

*Errors in azimuth and apparent velocity caused by errors in reading P-wave arrival times.*

Figure 9 shows a generalized tripartite array (A, B, C). The distance from A to B and the difference ( $T_A - T_B$ ) are defined as  $D_{AB}$  and  $T_{AB}$ , respectively; similarly for  $D_{AC}$  and  $T_{AC}$ .

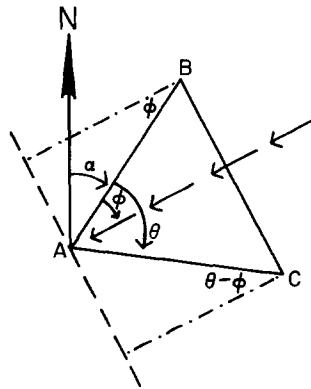


FIG. 9. A wave front (dashed line) is shown arriving at a tripartite array from a direction with azimuth  $\phi$  (referred to side AB). The array is oriented with side AB  $\alpha$  degrees from north. The dashed-dotted lines are used in the derivation of equation (1).

If the wave is assumed to have a planar wave front, then the azimuth ( $\phi$ ) and apparent velocity ( $V$ ) are as follows

$$\phi = \tan^{-1} \left( \frac{[D_{AB}T_{AC}/D_{AC}T_{AB}] - \cos \theta}{\sin \theta} \right) \tag{1}$$

$$V = \frac{D_{AB} \cos \phi}{T_{AB}} = \frac{D_{AC} \cos (\theta - \phi)}{T_{AC}} \tag{2}$$

The distance from the array is usually defined in this paper as the distance from the centroid of the array. In a few cases, it was found convenient to use one of the corners of the tripartite array as the origin. The  $S-P$  time used to determine distance is taken then as the average of all clearly read  $S-P$  times normalized to the centroid. Normalization can be achieved by subtracting or adding a time correction ( $TC$ ) to the arrival times;  $TC$  equals the perpendicular distance between a wave front arriving at the centroid and a wave front arriving at a given station divided by the product of 1.37 times the apparent velocity. The value of 1.37 is the ratio of  $S-P$  "velocity", defined as  $V_p V_s / (V_p - V_s)$ , to  $P$ -wave velocity assuming a Poisson's ratio of 0.25. Although this normalization is an approximation, its accuracy is sufficient in view of the relatively large errors in reading the  $S-P$  time discussed below.

If the array is surveyed with an accuracy of a few meters and care is taken to assure that no unpredictable timing errors are introduced during recording and playback, the only significant errors in equations (1) and (2) are errors in measuring the arrival time. Such errors depend on identification of the proper phase and the sharpness of onset. In practice, we find that the arrival times on the clearest records can be read with a relative precision of  $\pm 0.005$  sec if all data are recorded with the same time signal. Such a precision, which is surprisingly accurate for most seismologists studying earthquakes, is necessary for reasonably precise hypocentral locations determined with data from small arrays.

One common method of calculating the error in azimuth is to assume an error in  $T_{AB}$  and  $T_{AC}$  of  $\pm 2\Delta$  where the 2 is caused by errors ( $\Delta$ ) in reading  $T_A$  and  $T_B$  or  $T_A$  and  $T_C$ . This method is incorrect because the errors in measuring  $T_{AB}$  and  $T_{AC}$  are not independent. Errors calculated in this way are generally larger than the errors determined when the interdependence of timing errors is taken into account.

Differentiating equation (1) with  $T_{AC} = T_A - T_C$  and  $T_{AB} = T_A - T_B$ , the maximum error in the azimuth is

$$d\phi = \frac{\sin \theta D_{AB} D_{AC} [|T_C - T_B| dT_A + |T_A - T_C| dT_B + |T_A - T_B| dT_C]}{D_{AB}^2 (T_A - T_C)^2 - 2 \cos \theta D_{AC} D_{AB} (T_A - T_B)(T_A - T_C) + D_{AC}^2 (T_A - T_B)^2} \quad (3)$$

Two more equations identical in form to equation (3) can be written using different interior angles of the array.

The apparent velocity can be calculated in two ways for each internal angle (equation 2). The error equations have the form

$$dV_i = \frac{D_k (|\cos \phi_k| dT_i + dT_k) + (T_i - T_j) \sin \phi_k d\phi}{(T_i - T_j)^2} \quad (4)$$

where  $\phi_k$  is the angle from the  $k$ th side to the azimuth and where for three equations  $k = i$  and for three  $k = j$ . Only three errors are unique without regard to sign and these can be calculated with either  $k = i$  or  $k = j$ . All  $dV_i$  are not equal because  $T_i - T_j$  is in the denominator of the error equations. If  $T_i - T_j$  is small, a fixed, small error in  $T$  will cause a large error in  $V_i$  and  $dV_i$ .

The relationship of these various parameters is shown graphically in Figure 10. A point can be found on this graph for any three arrival times whose absolute differences ( $T_A - T_B$  and  $T_A - T_C$ ) are less than 0.2 sec. The azimuth, apparent velocity, and the maximum errors in azimuth and apparent velocity caused by a possible timing error of  $\pm 0.005$  sec at every station are estimated by interpolating between appropriate contours near this point. In practice, these errors can be readily calculated from equations (3) and (4) when the earthquake is located. Apparent velocity, as discussed below, can be related to distance. Therefore, the ellipses correspond to lines of equal distance from the array and the errors in azimuth and apparent velocity are nearly concentric with the ellipses. Thus, for an equilateral array, the errors are nearly constant at all azimuths for a given distance. The error in azimuth is slightly less at azimuths of  $30^\circ$ ,  $90^\circ$ ,  $150^\circ$  . . . , whereas the error in apparent velocity is slightly larger at these azimuths and less at azimuths which are integer multiples of  $60^\circ$ . If the array is not equilateral, the error contours rapidly become distorted and nonparallel to the apparent velocity or distance contours.

The errors shown in Figure 10 can be projected on a map by assuming a crustal structure such as structure D in Table 2. Contour maps of errors in azimuth, apparent velocity, distance, and depth for earthquakes at 3-km depth are shown in Figures 11 through 14 for an equilateral array assuming timing errors of  $\pm 0.005$  sec. Similar maps for a

scalene array are given by Ward and Björnsson (1971). In these figures, distances are measured from one arbitrarily chosen station in the array. The equilateral array has the most symmetric errors as a function of azimuth. If any interior angle of the array is greater than  $70^\circ$  or less than about  $50^\circ$ , the errors will change significantly with azimuth. Thus, the errors must generally be evaluated for each earthquake in order to discuss the precision of each hypocentral location.

Most workers using tripartite arrays have discussed the possible errors in the location of the earthquakes they studied. These discussions, however, have usually been minimal and have sometimes been incorrect. Maruyama and Kayano (1969) studied tripartite errors resulting from errors in reading arrival times by applying a Monte Carlo method

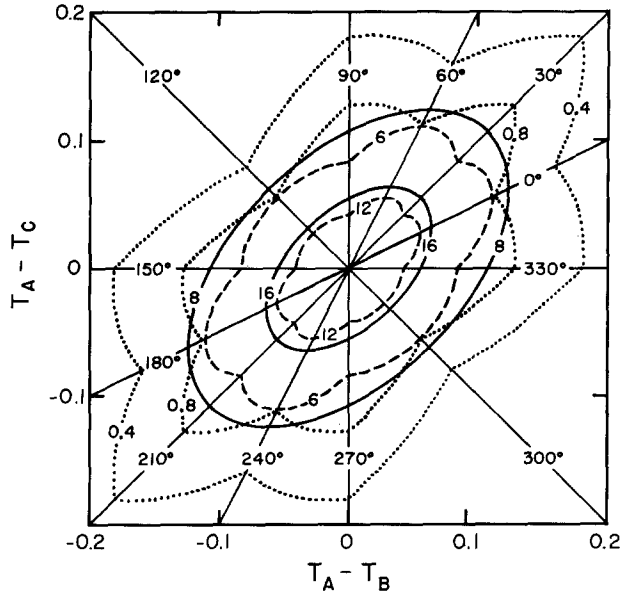


FIG. 10. Lines of equal azimuth (radial lines), apparent velocity (solid ellipses), error in azimuth (dashed multilobed curve), and error in apparent velocity (dotted multilobed curve) as functions of the arrival time differences  $T_A - T_B$  and  $T_A - T_C$  of an earthquake at an equilateral tripartite array with sides 1-km long.  $\alpha$  in Figure 9 is set equal to 0. The errors are calculated assuming possible errors of  $\pm 0.005$  sec in reading the  $P$  arrival times.

similar to that used in this paper to evaluate the precision of network locations and compared these results with analytical methods similar to those used here. Their results agree in principle with ours. The major difference is that, in this paper, the maximum error is calculated as a function of a given error in reading the arrival times, whereas Maruyama and Kayano (1969) stress the standard deviation of the errors and show how the standard deviation varies with azimuth. The method used here has the advantage that the error can be calculated by computer with a few short steps for each earthquake located. Maruyama and Kayano (1969) found that 300 or more samples must be averaged to show a statistically significant distribution of errors for the Monte Carlo method as they used it. In this paper, the errors are shown as a function of distance and depth of focus also. Ward and Björnsson (1971) observed 114 explosions from one source and found that in that particular case, the maximum errors as defined in this paper could be compared statistically to the 80 per cent confidence limits.

*Hypocentral locations for which a curved wave front is assumed.* For precise locations of earthquakes within distances of about 5 times the length of an average side of the array, it is unreasonable to assume a planar wave front—the main assumption of the apparent

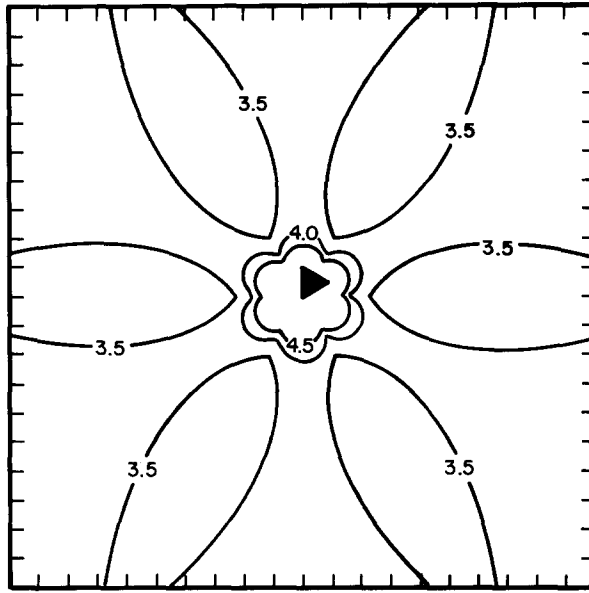


FIG. 11. Contour map showing the error in azimuth ( $\pm$  error in degrees) at the Earth's surface for events 3 km deep. The equilateral array is shown by the triangle. The grid is in kilometers. Point A of the array is the origin. The error is calculated assuming errors in reading the first arrivals at  $\pm 0.005$  sec. The crustal structure assumed in Figures 11 through 14 is that used by Ward and Björnsson (1971).

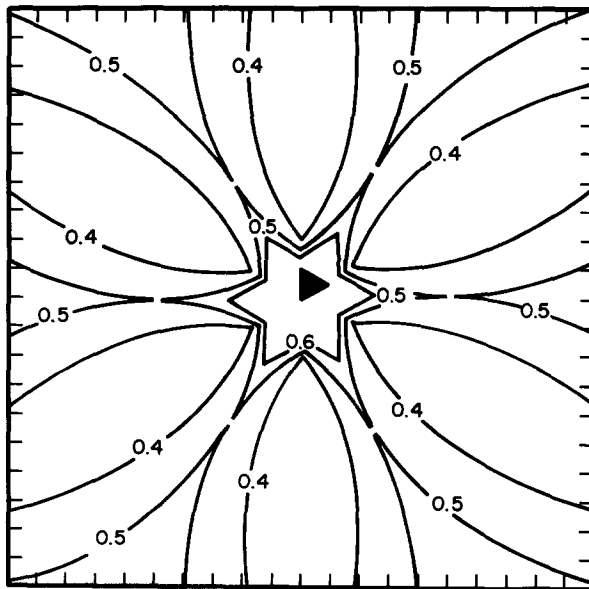


FIG. 12. Contour map showing error in apparent velocity ( $\pm$  error in km/sec) at the Earth's surface for events located at 3 km depth. The error is calculated assuming errors in reading the first arrivals of  $\pm 0.005$  sec. The grid is in kilometers.

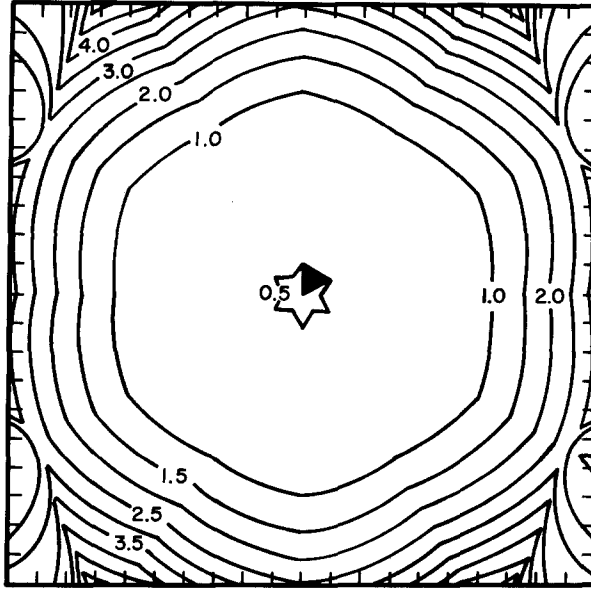


FIG. 13. Contour map showing error in distance from one corner of the array for events 3 km deep. The error is the maximum possible distance minus the least possible distance in kilometers. The grid is in kilometers. The errors are calculated assuming errors in reading the  $P$ -arrival times and  $S-P$  times of  $\pm 0.005$  and  $\pm 0.05$  sec, respectively.

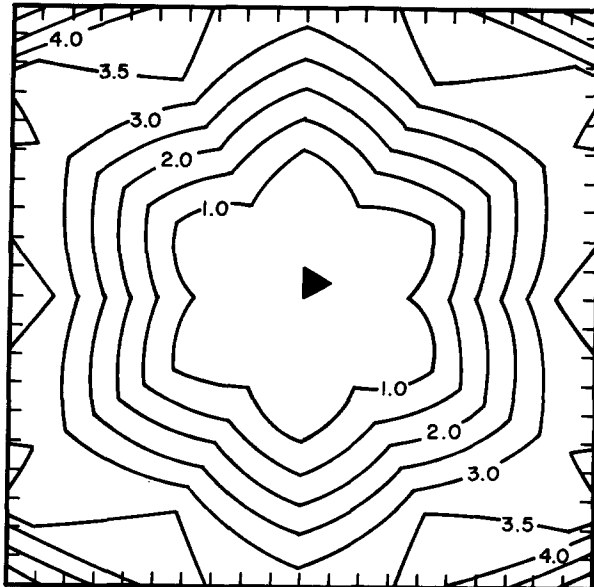


FIG. 14. Contour map showing error in depth for events 3 km deep. The error is the maximum possible depth minus the minimum possible depth. The errors are calculated assuming errors in reading  $P$ -arrival times and  $S-P$  times of  $\pm 0.005$  and  $\pm 0.05$  sec, respectively. The grid is in kilometers.

velocity and azimuth technique described to this point. Time corrections at each station can be derived to account for a curved wave front by first calculating the azimuth and distance assuming the planar wave front and then calculating a new azimuth and apparent velocity. Successive approximations are usually not necessary since the distance is primarily a function of the  $S-P$  time and the azimuthal corrections are small. To derive the time correction, let  $\tilde{A}$  be the vector from the hypocenter to the centroid of the array. Let  $\tilde{B}$  be the vector to station 1, 2 or 3. Then the difference in time ( $\Delta T$ ) for a curved instead of a planar wave front is

$$\Delta T = \frac{|B|}{V} \left[ 1 - \frac{\tilde{A} \cdot \tilde{B}}{|A||B|} \right] \quad (5)$$

where  $V$  is the apparent velocity. The error in the final location is now a more complicated function that is little different from the error calculated elsewhere in this paper because the corrections are small. The size of the corrections in azimuth and apparent velocity increases for events nearer the array or for a larger array. If an array is more than several kilometers across, a shallow event near one element of the array may have a direct upgoing first arrival with very high apparent velocity at that element but a critically refracted wave with another apparent velocity for a first arrival at the other stations. Then the wave front cannot be considered planar or spherical and the apparent velocity cannot be determined. To minimize such problems a tripartite array should have sides shorter than 3 to 5 km for locating local earthquakes by the apparent velocity and azimuth technique. Earthquakes near the array can be located by determining the origin time from the  $S-P$  intervals and using the three  $P$ -wave arrivals to calculate hypocentral coordinates by standard methods (e.g. James *et al.*, 1969).

*Solution for a tilted array.* The difference in elevation of the seismometers in the array must be taken into account when locating earthquakes if the plane of the array dips more than a few degrees. One method of correcting for the elevation is to subtract station corrections ( $\Delta T$ ) from the arrival times at stations B and C of the form

$$\Delta T = \frac{\Delta H}{V_p \sin \beta} - \frac{\Delta H}{V \tan \beta} \quad (6)$$

where

$$\beta = \cos^{-1} \frac{V_p}{V},$$

$\Delta H$  is the difference in elevation between stations B and A or C and A,  $V_p$  is the  $P$ -wave velocity of the first layer, and  $V$  is the apparent velocity. For steeply emerging rays, such as most of those in this study,  $\Delta T$  is close to  $\Delta H/V_p$ .

Another method is to calculate the azimuth and apparent velocity in the plane of the array and then recalculate the azimuth and apparent velocity in the horizontal plane. To do this, let  $\delta$  be an apparent dip and  $\rho$  be the true dip of a plane, then (Billings, 1954)

$$\tan \delta = \tan \rho \sin \alpha \quad (7)$$

where  $\alpha$  is the angle between the strike and the direction of apparent dip measured in the horizontal plane. Inasmuch as the two apparent dips of the sides of the array are known from surveying and the difference of the two  $\alpha$ 's must equal the angle between the two legs of the array,  $\alpha$  and  $\rho$  can be determined by solving the two simultaneous equations. The apparent dip in the direction of the earthquake can be calculated by using the azimuth calculated in the plane of the array as an approximation for  $\alpha$ . From the

definition of the dot product, it is possible to calculate the angle between the strike of the array plane and the horizontal component of the azimuthal vector in the array plane. Iteration improves the approximation for  $\alpha$ . The apparent velocity in the horizontal plane is

$$V = \frac{V_p}{\cos(\beta + \delta)} \quad (8)$$

Maruyama (1965) gives tables for the apparent velocity and azimuthal corrections for dips of up to  $10^\circ$ , which show that array tilts up to  $2^\circ$  can generally be ignored for precisions of less than  $3^\circ$  in azimuth and for waves with apparent velocities less than twice the velocity of the first layer.

*Problems with the usual procedure for the calculation of distance and depth for events outside the array.* Normally distance and depth for events outside the array have been calculated by assuming a crustal structure composed of a number of layers of constant velocity, calculating the angle of emergence

$$\beta = \cos^{-1} \frac{V_p}{V}, \quad (9)$$

where  $V_p$  is the velocity in the surface layer, and tracing the ray from layer to layer using Snell's law. The differences in time for an  $S$  wave and a  $P$  wave to traverse each layer are summed. The point in the structure reached by the ray when this sum equals the observed  $S-P$  time is considered the earthquake hypocenter. Many authors have constructed nomographs that allow them to find the depth and distance graphically. One such nomograph given by Hashizuma *et al.* (1965) (Figure 15) shows depth plotted against distance. Given an  $S-P$  time and apparent velocity, one can immediately find the corresponding distance and depth. This graphic method or a numerical method based on the principles outlined above gives reasonable hypocentral locations provided the first arrival at each seismometer in the array travels upward along the entire ray path from the earthquake and is not critically refracted. Given an  $S-P$  time and apparent velocity, it is impossible to tell how far a critically refracted wave will travel along an interface and to tell whether the earthquake is located on the interface or above it. At best, it is only possible to calculate a locus of distances and depths for a particular event.

Most seismologists using tripartite arrays to locate earthquakes either recognized this limitation or were fortunate in that none of their recorded first arrivals were critically refracted waves for the assumed crustal structure. Some authors did not take this limitation into account, however, and others tried to circumvent it improperly. For example, the critical distance ( $X_c$ ) at which the first arrival from an earthquake on the surface changes from the direct wave to the critically refracted wave is, for a two-layered model,

$$X_c = 2H[(V_2 + V_1)/(V_2 - V_1)]^{\frac{1}{2}} \quad (10)$$

where  $H$  is the thickness of the first layer and  $V_1$  and  $V_2$  are the velocities of the first and second layers, respectively. In the nomograph of Figure 15, the critical distance is 26.4 km for earthquakes at the surface and 13.2 km for earthquakes at the bottom of layer 1 (dashed line). Events occurring in the first layer and to the left of the critical distance line can be located uniquely. Events to the right of the line cannot. For layer 2, the critical distance is 85 km for events at 15-km depth and 168 km for events at 3-km depth. In this particular case, only a small part of the nomograph is in error. In the paper by Hashizume *et al.* (1965), however, nearly one third of the data have the appropriate apparent velocity and  $S-P$  time for events occurring in the first layer and to the right of the critical distance line. Therefore, much of their data cannot be used to support their

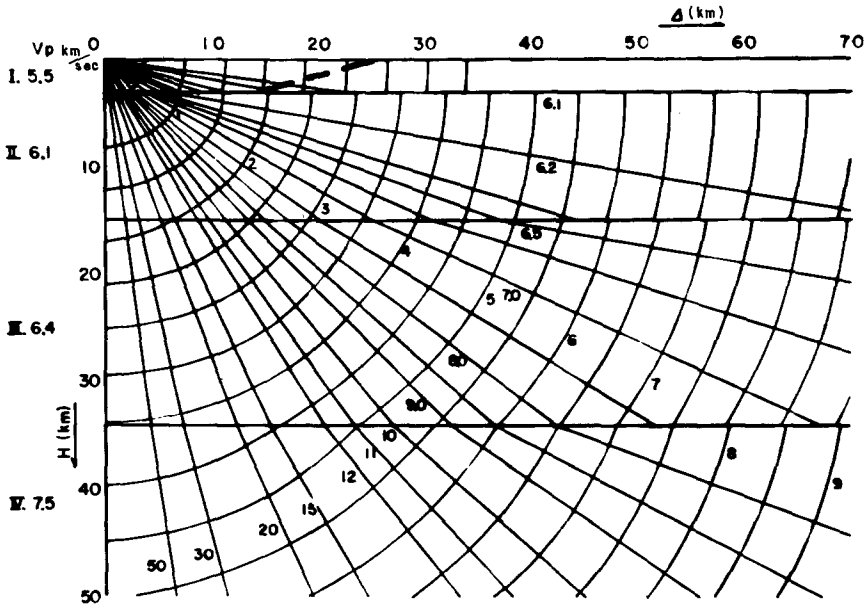


FIG. 15. Nomograph for graphically determining the distance and depth of an earthquake from apparent velocity and  $S-P$  time observed at a tripartite array (from Hashizume *et al.*, 1965). The radial lines are lines of equal apparent velocity in kilometers per second. The curves orthogonal to the apparent velocity lines are curves of equal  $S-P$  time in seconds. The dashed line was added by the present authors to show the critical distance versus depth in the first layer. The first arrivals from earthquakes to the right of this line in the first layer will be critically refracted waves.

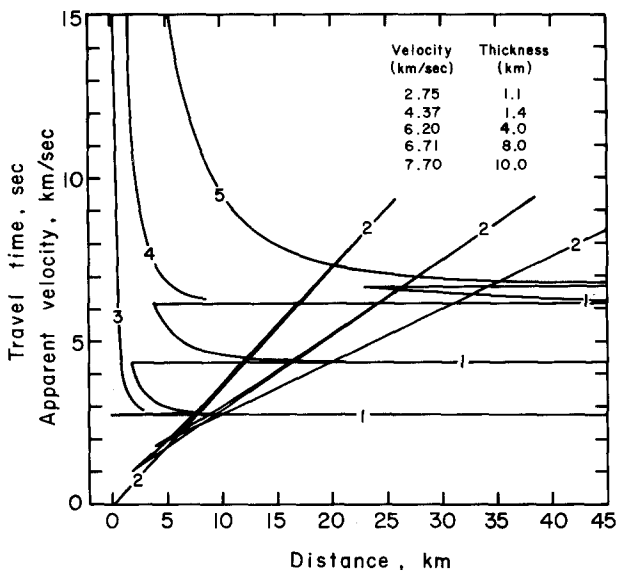


FIG. 16. Distance as a function of apparent velocity (curve 1) and travel time as a function of distance (curve 2) for the structure with layers of constant velocity shown and for earthquakes occurring at the surface. Curves 3, 4 and 5 show distance as a function of apparent velocity for earthquakes at depths 1, 2.5, and 10 km. Only the direct ray is considered in curves 3, 4, and 5.

conclusion that epicenters but not hypocenters can be fairly well determined with data from tripartite arrays.

Some authors (for example, Matumoto and Page, 1969, and Matumoto and Ward, 1967) tried to minimize the effect of the critically refracted wave by subdividing the crustal structure into a large number of layers, each less than 1 km in thickness. In this way, if a wave is not critically refracted along one of the layer boundaries, it will be reflected at such a high angle that it will travel nearly parallel to the boundary. Tracing critically refracted waves will still lead to nonunique solutions. The majority of the waves, however, will be reflected at very high angles and will return to the upper layers if the  $S-P$  time is sufficiently large. This method gives unique hypocenters for most earthquakes, but as shown below, can lead to a large scatter in the calculated hypocenters of events that actually occurred at a point.

A plot of distance and travel time versus apparent velocity is shown in Figure 16 for the crustal structure given in the figure. Distance is not a simple function of apparent velocity. Each horizontal line represents the velocity of one of the layers and is the apparent velocity corresponding to the critically refracted wave. In this crustal structure, critically refracted waves can only have velocities of 2.75, 4.37, 6.20 km/sec, etc. Each arcuate segment of curve 1 corresponds to a reflected wave, for which a slightly higher apparent velocity leads to a slightly smaller calculated distance. Generally, however, the apparent velocity increases for events at greater distances. Furthermore, the reflected wave is never the first arrival, although, as each layer is made thinner, the difference in arrival time between the first arrival and the reflected wave becomes smaller. Perhaps the worst feature of using a finely divided crustal structure is that, if the apparent velocity is nearly equal to the velocity of one of the layers, a small error in apparent velocity will lead to large errors in distance and depth. The wave may be reflected for one value of apparent velocity but transmitted into the next layer for a slightly higher apparent velocity. If the first arrivals were recorded for a large number of earthquakes with the same hypocenter, the scatter in the located hypocenters, assuming some error in reading the  $P$ -wave arrivals, would not only be a function of the error in reading but also a function of whether the mean observed apparent velocity happened nearly to equal the velocity of one of the layers. In practice, we have found that, even if each of the layers is 0.25 km thick, extremely small errors in apparent velocity (e.g.  $\pm 0.02$  km/sec) can cause errors in distance as great as 30 per cent of the calculated distance to an earthquake at the surface.

Thus, when a crustal structure with layers of constant velocity is assumed, the slope of the apparent velocity versus distance curve is not a smooth function. The error in distance caused by an error in reading first-arrival times is not a smooth function of distance near the cusps in the curve, and a large scatter of the calculated hypocenters may result at certain distances, even though the events occurred at a point.

For this reason, the data presented by Matumoto and Page (1969) and Matumoto and Ward (1967) should not be used in discussing fine-scale clustering of events outside the array or for correlating epicenters with anything other than large-scale surface features. Detailed conclusions should not be drawn from their cross sections showing the distribution of earthquakes with depth.

The assumption of a crustal structure with layers of constant velocity, as discussed above, can lead to nonunique hypocentral solutions and a large scatter in the hypocenters when the first arrivals are refracted waves. Curves 3, 4 and 5 in Figure 16 show distance as a function of apparent velocity where the hypocenters are at depths of 1 km, 2.5 km and 10 km, respectively. In these cases, only the wave traveling upward along the entire path between the hypocenter and array is considered. For this particular structure,

distance is sensitive to a small change in apparent velocity when the distance is less than about twice the depth. Beyond these distances, the first arrival is critically refracted and, therefore, the hypocenters can no longer be located uniquely.

*An improved method for calculating distance and depth for events outside the array.* By decreasing the thickness of each layer to zero and increasing the number of layers to infinity, that is, by introducing a few layers with gradients in velocity and removing first-order discontinuities in velocity, earthquakes at all distances can be located uniquely. The errors in distance and depth still depend on the error in apparent velocity, but they do not generally depend on the particular value of the apparent velocity. The scatter in hypocenters is, therefore, reduced.

From the equations given by Nettleton (1940), the time ( $T_i$ ) and distance ( $X_i$ ) in each layer are

$$T_i = [\cosh^{-1}(V/V_i) - \cosh^{-1}(V/V_{i+1})]/K_i \quad (11)$$

$$X_i = [(V^2 - V_i^2)^{\frac{1}{2}} - (V^2 - V_{i+1}^2)^{\frac{1}{2}}]/K_i \quad (12)$$

where the velocity gradient  $K_i = (V_{i+1} - V_i)/D_i$ , and  $V_i$  is the velocity at the top of the layer,  $V_{i+1}$  the velocity at the bottom of the layer and  $D_i$  the thickness of the layer.

If the  $S-P$  time is such that the ray stops going down in layer  $i$ , then

$$X_i = [(V^2 - V_i^2)^{\frac{1}{2}} - (V^2 - V_B^2)^{\frac{1}{2}}]/K_i \quad (13)$$

where

$$V_B = \frac{2VA \exp(-T_i K_i)}{A^2 \exp(-2T_i K_i) + 1}$$

and where

$$A = (V/V_i) + [(V^2/V_i^2) - 1]^{\frac{1}{2}}.$$

$T_i$  is the  $P$ -wave travel time in the layer. The depth in the layer where the ray ends, or in other words where the hypocenter occurs, is

$$H_i = (V_B - V_i)/K_i. \quad (14)$$

Curve 1 of Figure 17 shows the distance as a function of apparent velocity for such a crustal structure with velocity gradients within each layer and for earthquakes at the surface. In this case, distance is a monotonically increasing function of apparent velocity. A small change in apparent velocity causes a small change in distance until the ray reaches a layer with a small velocity gradient. Then very small changes in apparent velocity cause large changes in distance. Curve 2 shows the corresponding travel-time curve. Curves 3, 4 and 5 show distance as a function of apparent velocity for events at depths of 1.0, 2.5 and 10 km. Note that for this crustal structure, shallow earthquakes cannot be located very precisely at distances greater than about 8 km because of the low slope of the apparent velocity versus distance curve.

Figure 8 shows apparent velocities and travel time versus distance for the four different crustal structures and for earthquakes at the surface. Note that very small changes in the crustal structure can cause large changes in calculated distance. Curve 2 shows the apparent velocity versus distance for a structure where the velocity gradient is higher in layer 2 than in layer 1. Note that in this case three different apparent velocities can give the same distance over a narrow distance range. Only one of these three arrivals is the first arrival at a given distance, however. For example, if the assumed structure in this case is accurate, it is not theoretically possible to observe apparent velocities between 4 and 4.5 km/sec by studying the first  $P$ -arrivals from a surface-focus earthquake or explosion. For this

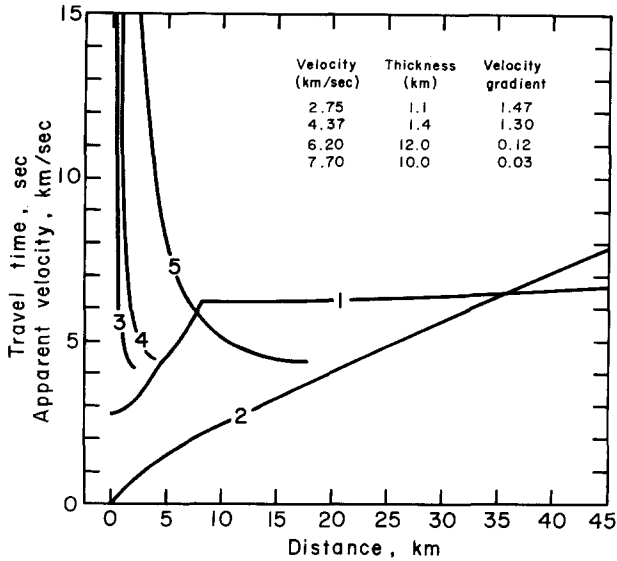


FIG. 17. Distance as a function of apparent velocity (curve 1) and travel time as a function of distance (curve 2) for the layered crustal structure with velocity gradients shown and for earthquakes occurring at the surface. Velocities given are velocities at the top of each layer. Curves 3, 4, and 5 show distance as a function of apparent velocity for earthquakes at depths 1, 2.5 and 10 km, respectively, where only the direct ray is considered.

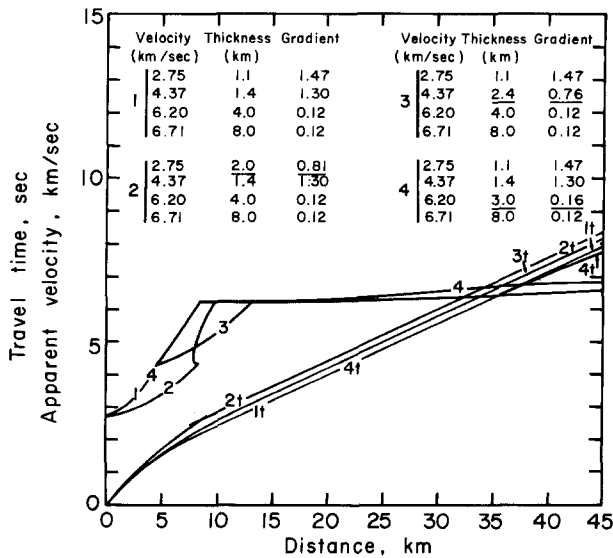


FIG. 18. Distance as a function of apparent velocity and travel time as a function of distance for the four slightly modified crustal structures shown. The underlined portion of each structure shows the change from structure 1.

reason, either the gradient should be assumed constant or monotonically decreasing with depth, or the calculated locations and errors in locations must be carefully examined at distances where there are cusps in the apparent velocity versus distance curves.

*Accuracy of hypocentral locations based on a crustal structure with velocity gradients.* By assuming a crustal structure with velocity gradients and no first-order discontinuities, hypocenters for earthquakes at all distances can be located more precisely. However, has the accuracy of these locations been improved? The accuracy is primarily determined by

how closely the assumed crustal structure approximates the actual structure. When reducing seismic refraction data, an effort is usually made to find the minimum number of layers of constant velocity that will fit the observed travel times. A crustal structure with a velocity gradient in each layer can usually be fit to the same first-arrival data but inversion is more difficult (Table 2). If limited data are available, this method does not normally give a unique solution. It is known from reflection surveys that the uppermost crust, at least, consists of more than a few layers with constant  $P$  velocities. Large changes in velocity across a thin boundary layer are certainly possible, as for example between two geological formations, but does this type of boundary prevail in the crust, particularly at depth? It should be possible to approximate the crustal velocity distribution as accurately by a large number of layers with gradients in velocity as by a few layers with constant velocities. Some sharp boundaries caused by phase changes or changes in metamorphism (Cann, 1968; Hess, 1962) seem to occur. A good example might be the Mohorovičić discontinuity (Kennedy, 1959). Both types of crustal structure, however, seem to give sufficiently accurate models for the locations of local earthquakes especially because both fit the available travel-time data.

*Accuracy of earthquake locations and station corrections.* Miyamura *et al.* (1962) found that azimuths recorded at two different arrays varied by as much as  $25^\circ$ . They explained these variations in terms of dipping crustal layers. Hashizume *et al.* (1965) compared solutions for four arrays operating simultaneously and found that the computed epicenters agreed within the precision but the focal depths did not. This suggests that their assumed crustal structure was in error or that the strike of any dipping crustal layers was nearly perpendicular to the ray paths. An additional problem in their method of determining hypocenters was discussed above. Stauder and Ryall (1967) showed that station corrections for travel-time delays caused by variations in surface geology under the array can amount to as much as 0.11 sec in extreme cases for an array with sides of about 1.5 km. Such a large correction at one corner of an array of this size, if not taken into account, would cause most of the events to be located in a narrow azimuth range regardless of their true azimuth. Ward and Björnsson (1971) found that explosions in Iceland at distances less than 10 km could be located accurately using an array with 1-km sides. At greater distances, however, errors as large as  $38^\circ$  in azimuth and a factor of 1.8 in apparent velocity were found. Most of these errors could be explained by assuming station corrections of less than 0.05 sec. These corrections could be caused by one layer dipping  $2^\circ$  to  $5^\circ$ . Calibration explosions or some independently located earthquakes are needed to determine the accuracy of the earthquake locations. These calibration events should be placed at a large number of different azimuths and distances near hypocenters of events located by the array.

#### REFERENCES

- Aki, K. (1962). Study of earthquake waves by seismometer array. Part 1. Aftershocks of the Kitamino earthquake of August 19, 1961, *Bull. Earthquake Res. Inst., Tokyo Univ.* **40**, 371–389 (In Japanese).
- Aki, K., and H. Matumoto (1963). Study of earthquake waves by means of a seismometer array. Part 2. A study of the crustal structure in the Kanto region by the observation of apparent velocity of  $P$ -waves caused by many small earthquakes, *Bull. Earthquake Res. Inst., Tokyo Univ.* **41**, 279–292 (In Japanese).
- Anderson, O. L. and R. C. Liebermann (1966). Sound velocities in rocks and minerals, *VESIAC State-of-the-Art Report 7885-4-X*, Willow Run Laboratories, 182 p.
- Asada, T. and Z. Suzuki (1950). On microearthquakes observed after the Imaichi earthquake, December 26, 1949, *Bull. Earthquake Res. Inst., Tokyo Univ.* **28**, 415–421.
- Billings, M. P. (1954). *Structural Geology*, Prentice-Hall, New York, p. 443.
- Cann, J. R. (1968). Geological processes at mid-ocean ridge crests, *Geophys. J.* **15**, 331–341.

- Crow, E. L., F. A. Davis, and M. W. Maxfield (1960). *Statistics Manual*, Dover, New York.
- Dieterich, J. H. (1972). Numerical modeling of deformations associated with volcanism, *Geol. Soc. Am. Abstracts with programs*, **4**, 146.
- Draper, N. R., and H. Smith (1966). *Applied regression analysis*, John Wiley and Sons, New York.
- Eaton, J. P. (1962). Crustal structure and volcanism in Hawaii, *Crust of the Pacific Basin, Geophys. Monograph* **6**, 13–29.
- Eaton, J. P. (1969). HYPOLAYR—a computer program for determining hypocenters of local earthquakes in an earth consisting of uniform flat layers over a half-space, *U.S. Geological Survey Open File Report*.
- Eaton, J. P., M. E. O'Neill and J. N. Murdock (1970). Aftershocks of the 1966 Parkfield-Cholame, California, Earthquake: A detailed study, *Bull. Seism. Soc. Am.* **60**, 1151–1197.
- Endo, E. T. (1971). Focal mechanism for the May 15–18, 1970, shallow Kilauea earthquake swarm, *M.S. Thesis*, San Jose State College, San Jose, California.
- Fiske, R. S. (1969). Anatomy of an active volcano—Kilauea 1965–68, *Trans. Am. Geophys. Union* **50**, 113.
- Geiger, L. (1912). Probability method for the determination of earthquake epicenters from arrival time only. *Bull. St. Louis University*, **8**, 56–71.
- Gorshkov, G. S. (1971). Prediction of volcanic eruptions and seismic methods of location of magma chambers—a review, *Bull. Volcanol.* **35**, 198–211.
- Hamilton, R. M. and J. H. Healy (1969). Aftershocks of the BENHAM nuclear explosion, *Bull. Seism. Soc. Am.* **59**, 2271–2281.
- Hashizume, M., K. Oike, and Y. Kishimoto (1965). On the accuracy of the tripartite method, *Bull. Disaster Prev. Res. Inst.* **15**, 7–29.
- Hess, H. H. (1962). History of ocean basins, in *Petrologic Studies—A Volume in Honor of A. F. Buddington*, A. E. J. Engel, H. L. James, and A. F. Buddington, Editors, Geological Society of America, 599–620.
- Hill, D. P. (1969). Crustal structure of the island of Hawaii from seismic-refraction measurements, *Bull. Seism. Soc. Am.* **59**, 101–130.
- James, D. E., I. S. Sacks, E. Lazo L., and P. Aparacio G. (1969). On locating local earthquakes using small networks, *Bull. Seism. Soc. Am.* **59**, 1201, 1212.
- Kennedy, G. C. (1959). The origin of continents, mountain ranges, and ocean basins, *American Scientist* **47**, 491–504.
- Koyanagi, R. Y., H. L. Krivoy, and A. T. Okamura (1966). The 1962 Koaiki, Hawaii, earthquake and its aftershocks, *Bull. Seism. Soc. Am.* **56**, 1317–1335.
- Lee, W. H. K. (1970). HYPO70 (Version I): A computer program for determining hypocenter, magnitude, and first motion pattern of local earthquakes, *U.S. Geological Survey Open-File Report*.
- Lee, W. H. K. and J. C. Lahr (1971). HYPO71: A computer program for determining hypocenter, magnitude, and first motion pattern of local earthquakes, *U.S. Geological Survey Open-File Report*.
- Manghnani, M. H. and G. P. Woolard (1968). Elastic wave velocities in the Hawaiian rocks at pressures of ten kilobars in *The Crust and Upper Mantle of the Pacific Area*, American Geophysical Union, *Geophys. Monograph* **12**, 501–516.
- Maruyama, T. (1965). Slope corrections in tripartite net observations, *Bull. Earthquake Res. Inst., Tokyo Univ.* **43**, 409–420 (In Japanese).
- Maruyama, T. and I. Kayano (1969). Errors in apparent velocity and direction of approach determined by the tripartite net observation of a seismic signal, *Bull. Earthquake Res. Inst., Tokyo Univ.* **47**, 571–598 (In Japanese).
- Matumoto, T. (1959). Tesikaga earthquake of January 31, 1959, *Bull. Earthquake Res. Inst., Tokyo Univ.* **37**, 531–544 (In Japanese).
- Matumoto, T. (1971). Seismic body waves observed in the vicinity of Mount Katmai, Alaska, and evidence for the existence of molten chambers, *Bull. Geol. Soc. Am.* **82**, 2905–2920.
- Matumoto, T. and R. A. Page, Jr. (1969). Microaftershocks following the Alaska earthquake of March 28, 1964: Determination of hypocenters and crustal velocities in the Kenai Peninsula–Prince William Sound Area. *The Prince William Sound, Alaska, Earthquake of 1964 and Aftershocks, Vol. II, Parts B & C*, ESSA, CGS Publ. 10–3, 157–173.
- Matumoto, T. and P. L. Ward (1967). Microearthquake study of Mt. Katmai and vicinity, Alaska, *J. Geophys. Res.* **72**, 2557–2568.
- Mikumo, T. (1965). Determination of phase velocity and direction of wave approach from station arrays, *Bull. Disaster Prev. Res. Inst.* **15**, 31–45.

- Minakami, T. (1960). Fundamental research for predicting volcanic eruptions (Part 1), *Bull. Earthquake Res. Inst., Tokyo Univ.* **38**, 497–544.
- Minakami, T. (1964). The 1962 eruption of Miyake-Shima, one of the seven Izu Islands, *Bull. Volcanol. Soc. Japan* **27**.
- Miyamura, S., M. Hori, K. Aki, M. Tsujiura, and H. Matumoto (1962). Simultaneous operation of two seismometer array stations in a study of microearthquakes in the Kanto and Chubu region, *Bull. Earthquake Res. Inst., Tokyo Univ.* **40**, 885–897 (In Japanese).
- Miyamura, S., M. Hori, H. Matumoto, and M. Tsujiura (1964). Observation of microearthquakes by a seismometer array at Hachiman, Gifu Prefecture, Central Japan, *Bull. Earthquake Res. Inst., Tokyo Univ.* **42**, 257–272 (In Japanese).
- Moore, J. G. and H. L. Krivoy (1964). The 1962 flank eruption of Kilauea Volcano and structure of the east rift zone, *J. Geophys. Res.* **69**, 2033–2045.
- Nersesov, I. L. and T. G. Rautian (1960). Chapter 3: Structure of the Earth's crust and analysis of seismic observations in *Methods of the detailed study of seismicity*, Riznichenko, Editor, *Trudy Inst. Fis. Zemli*, **9**, 30–74.
- Nettleton, L. L. (1940). *Geophysical Prospecting for Oil*, McGraw-Hill, New York, p. 256.
- Ohtake, M., T. Asada, and S. Suyehiro (1965). A distorted distribution of apparent velocities observed with ultrasensitive tripartite network, *Zisin* **18**, 15–24 (In Japanese).
- Oike, K. and T. Mikumo (1968). Seismometer array method for the observation of microearthquakes in relation to local underground structure, *Zisin* **21**, 54–66 (In Japanese).
- Okamura, A. T., R. Y. Koyanagi, and W. T. Kinoshita (1969). *Hawaiian Volcano Observatory Summary* 47: July, August, and September 1967.
- Otsuka, M. (1966). Azimuth and slowness anomalies of seismic waves measured on the central California's seismographic array, Part II, Interpretation, *Bull. Seism. Soc. Am.* **56**, 655–675.
- Ryall, A. and D. L. Bennett (1968). Crustal structure of southern Hawaii related to volcanic processes in the upper mantle, *J. Geophys. Res.* **73**, 4561–4582.
- Stauder, W. and A. Ryall (1967). Spatial distribution and source mechanism of microearthquakes in central Nevada, *Bull. Seism. Soc. Am.* **57**, 1317–1346.
- Swanson, D. A., W. A. Duffield, and R. T. Okamura (1971). Seaward displacement of the south flank of Kilauea Volcano, *Trans. Am. Geophys. Union* **52**(4).
- Wada, T. and Y. Sudo (1967). Focal mechanism of volcanic earthquakes of the volcano Aso, *Bull. Volcanol. Soc. Japan* **12** (In Japanese).
- Walker, G. W. (1969). Geologic map of the Kau Desert Quadrangle maps of the United States, U.S. Geological Survey Map GQ-827.
- Ward, P. L., and S. Björnsson (1971). Microearthquakes, swarms, and the geothermal areas of Iceland, *J. Geophys. Res.* **76**, 3953–3982.
- Wesson, R. L. (1971). Earthquake location in structurally complex models, *Trans. Am. Geophys. Union*, **52**, 284.
- Zobin, V. M. (1970). The mechanism of the volcanic earthquakes connected with the eruption of the volcano Sheveluch in November, 1964, *Izv., Earth Physics, No. 3, A.G.U. Translations*, 161–164.

U.S. GEOLOGICAL SURVEY  
NATIONAL CENTER FOR EARTHQUAKE RESEARCH  
MENLO PARK, CALIFORNIA 94025

LAMONT-DOHERTY GEOLOGICAL OBSERVATORY  
OF COLUMBIA UNIVERSITY  
PALISADES, NEW YORK 10964  
CONTRIBUTION NO. 1944

Manuscript received October 2, 1972